AMERICAN UNIVERSITY OF BEIRUT

THE DESIGN AND TESTING OF A MAXIMUM POWER POINT CONTROLLER FOR A LARGE PV GENERATOR UNDER NONUNIFORM IRRADIANCE

by
FARAH MAHMOUD KAZAN

A thesis
submitted in partial fulfillment of the requirements
for the degree of Master of Engineering
to the Department of Electrical and Computer Engineering
of the Faculty of Engineering and Architecture
at the American University of Beirut

Beirut, Lebanon
April 2014

AMERICAN UNIVERSITY OF BEIRUT

THE DESIGN AND TESTING OF A MAXIMUM POWER POINT CONTROLLER FOR A LARGE PV GENERATOR UNDER NONUNIFORM IRRADIANCE

by
FARAH MAHMOUD KAZAN

Approved by:

_____
Dr. Sami Karaki, Professor   Advisor
Electrical and Computer Engineering

_____
Dr. Rabih Jabr, Associate Professor   Co-Advisor
Electrical and Computer Engineering

_____
Dr. Mohammad M. Mansour, Associate Professor   Member of Committee
Electrical and Computer Engineering

Date of thesis defense: April 28, 2014

AMERICAN UNIVERSITY OF BEIRUT

THESIS, DISSERTATION, PROJECT RELEASE FORM

Student Name: _____Kazan_____Farah_____Mahmoud___
                     Last   First   Middle

◯ Master's Thesis   ◯ Master's Project   ◯ Doctoral Dissertation

☐   I authorize the American University of Beirut to: (a) reproduce hard or electronic copies of my thesis, dissertation, or project; (b) include such copies in the archives and digital repositories of the University; and (c) make freely available such copies to third parties for research or educational purposes.

☐   I authorize the American University of Beirut, **three years after the date of submitting my thesis, dissertation, or project,** to: (a) reproduce hard or electronic copies of it; (b) include such copies in the archives and digital repositories of the University; and (c) make freely available such copies to third parties for research or educational purposes.

_____

Signature   Date

ACKNOWLEDGMENTS

AN ABSTRACT OF THE THESIS OF

Farah Mahmoud Kazan   for   Master of Engineering
                               Major: Electrical Engineering

Title: The Design and Testing of a Maximum Power Point Controller for a Large PV
Generator under Nonuniform Irradiance

A Photovoltaic array (PV) has a current-voltage characteristic curve with a
maximum power point (MPP) that varies with changing atmospheric conditions, i.e.
solar radiation and temperature. An important consideration in the design of an efficient
PV system is its ability to correctly track the MPP as the atmospheric conditions vary.
The thesis presents a new method for maximum power point tracking, which combines
Ripple Correlation and Incremental Conductance, in a system consisting of a
photovoltaic generator, a boost converter, and their associated control. The method
relies on the natural disturbance created by the switching operation of the converter, and
on estimating the incremental and average conductance values of the PV generator
output. It is based on a characteristic property which stipulates that the incremental and
average inductances have the same absolute values at the MPP. Thus when operating at
a voltage point higher than that of the MPP, the absolute incremental conductance is
higher than the absolute average conductance and so the duty cycle of the converter
needs to be increased. The required change in the duty cycle is obtained using a digital
proportional-integral-derivative (PID) controller that aims to equalize the average and
incremental inductances. A system simulation model from first concepts was developed
in MATLAB taking into consideration implementation details of voltage and current
measurements and the presence of a junction capacitance.

The characteristics get more complicated if the array does not receive uniform
irradiance, which results in multiple peaks. The non-uniform irradiance in large PV
arrays is attributed to partially shaded PV modules and may significantly increase the
complexity of the MPP tracking problem to track the global peak without getting stuck
at a local one. The thesis introduces a novel two-stage approach for tracking the
maximum power point of a large photovoltaic generator under non-uniform irradiance.
In Stage 1, the method makes use of real-time irradiance measurements in certain
regions of the generator's panels to estimate the total power versus voltage (P-V) curve
and to deduce an estimate of the global peak region. This is followed in Stage 2 by the
single peak tracking approach to accurately locate the exact global power point. The
system consists of a PV generator, with pyranometers distributed across it, a DC-DC
converter feeding a battery, and a controller implementing the tracking algorithm. The
system simulation model was developed in MATLAB, taking into consideration the
implementation of bypass and blocked diodes together with the pyranometer irradiance
inputs.

CONTENTS

ILLUSTRATIONS

TABLES

CHAPTER I

INTRODUCTION

1.1. General Overview

The world demand for electric energy is constantly increasing and conventional fossil fuel energy resources are diminishing and are even threatened to be depleted. Moreover, they are major contributors to atmospheric pollution and global warming and their prices are rising. For these reasons, the need for alternative energy sources has become indispensible and renewable energy is a new trend in clean energy production, which includes power generated from water, wind, solar radiation, biomass, and other resources. This development of renewable power sources will save fossil fuel resources, and help improve the quality of the environment. One of the most prominent renewable energy sources is electric energy from the sun through photovoltaic (PV) arrays; it has great potential because it makes use of the most abundant energy on earth [1]. Solar energy in particular has proved to be a very promising alternative due to its availability and pollution-free nature. The freely and abundantly available solar energy can be easily converted into electrical energy using the PV cells. However, a major problem in PV systems arises in that their efficiency is still relatively low, and their performance depends on temperature, solar irradiance, array configuration, and shading. Moreover, multiple power peaks appear when PV panels are submitted to partial shading, hence, the need to track the global peak among the local ones. So, the maximum power point (MPP) must be continuously tracked as environmental conditions change, for the PV system design to be quite efficient.

A PV array has a current-voltage characteristic curve with a maximum power point that varies with changing atmospheric conditions, i.e. solar radiation and temperature. In fact, the amount of electric power generated by PV panels is always changing with weather conditions. Thus, a major challenge in using a PV source is to tackle its nonlinear characteristic of power versus voltage, which results in a unique MPP which needs to be tracked when weather conditions change. An important consideration in the design of an efficient PV system is its ability to correctly track the MPP as the temperature and solar radiation vary. Research on maximum power point tracking (MPPT) started in 1968 to improve the energy efficiency of PV power generation, specifically for space applications. The characterization of the maximum power point for modules working under varying irradiance is well established and several control algorithms have been proposed for tracking single peak curves. The most prominent are the perturb and observe (P&O) algorithm [2], the incremental conductance (IC) method [3], and the ripple correlation control (RCC) method [4,5].

The characteristics get more complicated if the array does not receive uniform irradiance, which results in multiple peaks [6]. Often, the PV arrays get shadowed, completely or partially, by passing clouds, neighboring buildings, towers, trees, and utility and telephone poles. When multiple PV modules are under non-uniform irradiance levels, the characteristic power-voltage curve features several local maxima and the usual MPPT methods can leave the operation stuck in a local maximum. The presence of multiple peaks reduces the effectiveness of the existing MPP tracking schemes that assume a single peak point due to their inability to discriminate between local and global peaks. Nevertheless, it is very important to understand and predict the PV characteristics in order to use a PV installation effectively under all conditions and

to apply efficient techniques that track the global peak without getting stuck at a local one.

1.2. Thesis Scope of Work and Significance

The scope of work of this thesis first includes proposing a new method for maximum power point tracking that makes use of both methods: IC and RCC. The method relies on the natural disturbance created by the switching operation of the converter, and on estimating the incremental and average conductance values of the PV generator output. The error of the actual operating point at each sampling time is calculated based on the fundamental concept of IC, namely that $\Delta P/\Delta V$ at the MPP is zero. However, the presented method does not evaluate the changes in the current and voltage values from the present and previous samples as in the IC method. Instead, it makes use of the panel's inherent current and voltage ripples caused by the boost converter without artificial and intentional perturbation at each sampling time. A system simulation model from first concepts was developed in MATLAB taking into consideration implementation details of voltage and current measurements and the presence of a junction capacitance.

The second issue that the thesis deals with is the approach for computing the I-V and P-V characteristics of an array under partial shading. The thesis presents a model for a large PV array taking into account the temperature, sun's irradiance, and partial shading factors, to depict its current-voltage and power-voltage characteristic curves. This enables the dynamics of a PV system to be easily simulated and later optimized. A MATLAB-based modeling and simulation scheme suitable for studying the I–V and P–

V characteristics of a PV array under non uniform irradiance due to partial shading was developed.

The third problem on which the thesis is focused is the problem of tracking the MPP in case of multiple peaks. The thesis introduces a novel two stage approach for tracking the MPPT for panels under partial shading. In stage one, an estimation of the characteristic curves is done based on few pyranometers distributed along the panel for the measurement of irradiance levels. The peak of the estimated curve would normally lie in the region of the global peak and makes a good starting operating point for stage 2. Then, in stage 2 a single MPPT method [7] is employed to accurately track the global peak. The advantage of this method is that it does not perturb the operation by carrying out open circuit and short circuit tests in trying to localize the global peak. The system simulation model was developed in MATLAB, taking into consideration the implementation of bypass and blocked diodes together with the pyranometer irradiance inputs.

1.3. Thesis Organization

This thesis is organized as follows: Chapter 2 presents a literature review on most common MPPT algorithms for tracking single and multiple peak curves and on the modeling of PV generators under non uniform irradiance. Chapter 3 presents a novel single peak tracking method. It presents the theory of MPP operation according to this method, the models of the different subsystems used in the simulation, and the implementation details of the PID controller as well as results on the tracking efficiency under various irradiance profiles. Chapter 4 presents a modeling and simulation scheme suitable for studying the I-V and P-V characteristic curves of a PV array with partial

shading configuration, given the exact irradiance values. Chapter 5 presents a method of

global peak region estimation knowing the readings and the location of the distributed

pyranometers. Tracking results of the two-stage approach are demonstrated under

various shading configuration cases. Chapter 6 concludes this work and proposes future

tasks to be tackled.

CHAPTER II

LITERATURE REVIEW

This chapter reviews the literature on methods of MPPT for single and multiple power peak curves and on the characterization of P-V curves for photo-voltaic generators under non uniform irradiance levels.

2.1. MPPT Techniques for Single Power Peak Curves

Many methods have been proposed to introduce new approaches for dealing with MPP tracking for single peak curves. The general objective is the same; what differs is the control idea to tackle the problem concentrating on a certain aspect. Some aim to make the system less expensive and complicated, others make use of approximations and assumptions related to PV behavior to make the algorithm simpler; still others concentrate on the problem of tradeoff between efficiency and tracking speed. Here is brief description of some of the most known approaches.

The perturb and observe (P&O) method [2] searches for the MPP on a power-voltage curve by comparing its sampled power and voltage with their previous values. As long as the power variation (ΔP) is positive, the operating voltage is kept being perturbed in the same sense. Once the power decreases, the sense of perturbation is inverted. The operating voltage of the panel is controlled by duty cycle variation of a DC-DC converter connected between the panel and the load. The main advantage of the P&O method is its ease of implementation [1]. However, its disadvantages include oscillation around the MPP thus causing power losses and lack of accuracy at steady state. Moreover, there is a tradeoff between convergence speed and steady state

oscillations because of the fixed step size perturbation at any iteration. The P&O method exhibits slow convergence to the MPP when small steps are taken and wide oscillations around the MPP in case of large steps. Another drawback is that it may fail to track the MPP as environmental conditions rapidly change.

An enhancement to the classical P&O method was the dP-P&O method [8] to improve its performance by preventing wrong direction tracking in case environmental conditions suddenly and rapidly fluctuated. Indeed if an irradiance change occurred during the sampling period, the resulting ΔP due to complete change in the P-V curve may be misleading. This approach uses an additional measurement taken in the middle of a sampling period to calculate the change in power dP due to pure tracking perturbations and separate it from a change due to environmental change dP_2. However, in case of fast changing conditions, the approach assumes that the voltage at the MPP increases with a rise in irradiance and accordingly increases V_{ref}. But, this assumption is not always valid as the opposite may occur at high irradiance due to the panel's series resistance.

Another well-known algorithm is the incremental conductance (IC) method [3] which is based on the fact that the incremental and average inductances have the same absolute value at the MPP, where $dP/dV = 0$ or $\Delta I/\Delta V = -I/V$. At each sampling period, present and previous values of V and I are measured to compute ΔV and ΔI and check whether the MPP condition is reached. If $\Delta I/\Delta V < -I/V$, the operating voltage is at the right of the peak and the duty cycle for the next iteration is increased by a predetermined fixed step ΔD. The opposite is true if $\Delta I/\Delta V > -I/V$. Oscillations around the MPP at steady state are reduced as compared to those in the classical P&O method, but they still occur since the slope of P versus V curve does not reach zero. Also, a

compromise between accuracy and convergence speed should be decided if the perturbation size is fixed. Hussein et al [3] argue that the IC technique is better than the P&O method under rapidly changing atmospheric conditions; tests results in [3] showed that the efficiency of the power extracted from a PV array using the IC algorithm (89.9%) is higher than that of the P&O algorithm (81.5%).

To solve the speed-accuracy tradeoff problem, an approach for automatically tuning the step size has been proposed in references [9] and [10] for P&O and IC tracking respectively. The duty ratio step size is varied and determined by the expression $\pm N*(\Delta P/\Delta V)$. The derivative of power with respect to voltage (dP/dV) after proper scaling acts as a good tuning for the duty ratio step size, which is quite large when away from the MPP and decreases when approaching the peak from either side. To ensure convergence, the scaling factor N is also automatically tuned at the starting-up process after perturbing the system with a maximum desired step ΔD_{max} and measuring the corresponding changes in power ΔP_{max} and voltage ΔV_{max}. N is defined such that it is less than $\Delta D_{max}*(\Delta V_{max}/\Delta P_{max})$.The limitation of this approach is that $\Delta P/\Delta V$ may reflect a correct measure from the maximum only if irradiance conditions are constant or slightly varying. But, under rapidly fluctuating conditions, the approach may not be practical. Also, a simplifying approximation is that $\Delta P_{max}/\Delta V_{max}$ is assumed uniform regardless of the initial position at the initialization prior to perturbation. Fig.1 of ref [11] shows how this assumption is not true. Quing Mei et al [12] also mention that the fixed scaling factor N becomes impractical when conditions change significantly or rapidly and thus would not be suitable for different P-I curves. A solution for this problem in [12] was to use the product of the power and its slope ($C=P*dP/dI$) to represent step sizes according to four different modes. First, $\Delta C/\Delta I$ and $\Delta V/\Delta I$ are

computed to determine whether the operating point is on the left or right of the MPP (by comparing $\Delta V/\Delta I$ with $-V/I$). Then depending on the sign of $\Delta C/\Delta I$, it is decided whether a fixed or variable step size should be applied. The variable step size S_k for perturbing the reference current is not a function of the scaling factor anymore, instead a function of $\sin(\varphi_k)=\mathrm{f}(dP/dI)$, which becomes very small when approaching the MPP.

Apart from the classical P&O and IC methods, a more recent approach known as ripple correlation control (RCC) tracks the MPP without artificial and intentional perturbations at each sampling period [4-5]. Instead it takes advantage of the naturally inherent ripples observed in the panel's voltage, current, and power signals caused by circuit switching in the DC-DC boost converter. The RCC method correlates the time varying PV array power with the time varying array current or voltage. Thus, if the array current is increasing and the power is also increasing then the time derivatives of power and current are both positive, and thus their product is positive. This indicates that the operating point is to the left of the MPP and hence the module voltage needs to be increased or its duty cycle reduced. The opposite is true if ripples are out of phase. With an integral feedback control to reach steady-state with $dp/di = 0$, the duty ratio D is adjusted according to the control law $k\int (dp/di)dt$. However, differentiating p with respect to i is difficult to implement in practical circuits and therefore a better control approach would be $k\int (dp/dt)\,(di/dt)\,dt$. The main advantage of RCC includes the utilization of the ripple available in the power electronic converter instead of using external perturbation. The method converges asymptotically with a fast rate to the MPP and no assumptions of the PV behavior or characteristics are used. However, a problem in this method is in the complexity of implementing circuit designs for signal differentiation. The approach in this thesis, as explained later in chapter III, differs in

that it also makes use of the inherent current and voltage ripples caused by the boost converter, but computes the error and changes the duty cycle accordingly by an implemented PID controller that aims to bring the offset error e to zero. The PID controller is easier to implement in the circuit designs.

Kimball and Krein [5] extended the analog RCC method to the discrete digital domain. Their method is known as discrete-time RCC or DRCC in which signals are sampled and measured just at certain times sufficient for suitable duty cycle adjustment calculations. By approximating the slopes of i and v as constant during each on-off switch mode, only two samples per switching period at the transient switching between the on and off states are sufficient to determine ΔD. This digital implementation and reduction in sampling makes the system simpler, less expensive, and less power consuming. Reference [5] also discusses the array capacitance effect that causes the panel current to be different than the measured inductor current. They introduce a phase shift in the measured coil current relative to the actual PV current and propose a solution to compensate such capacitance effect by correlating power with voltage instead of current.

Another adjustment to the approach of RCC by Kroeger et al [13] introduces the notion of digital implementation of a continuous-time RCC using DSP with an interface board, to treat analog signals received by the DSP. A DRCC is implemented on SIMULINK and the RCC control law of duty cycle is discretized to function on the DSP with a discrete time integrator and ripple correlator of p and i. Moreover, the array's capacitance effect is eliminated with a phase compensator for the phase shift induced in the inductor current.

2.2. Characteristic Curves of PV modules

Many researchers have studied the characteristic curves of PV modules and the factors affecting them. Walker [14] proposed a MATLAB-based simulation of the characteristics of a PV module to study the effect of temperature, irradiance and load variation on the output power. But his model does not consider the effect of shading on the characteristics. In [15], the I-V curves of the PV module were experimentally obtained to study the effect of partial shading; however the work is limited to a module level study and does not take into consideration an entire PV array. Similarly, Kawamura et al. [16] have also detected the change in the I-V characteristic curves of PV modules due to partial shading. Single PV modules whose characteristic curves do not show the presence of multiple peaks observed for large PV arrays receiving nonuniform irradiance were considered in their study. Patel and Agarwal in [6] proposed a MATLAB-based code that simulates the characteristics of a PV array with partial shading.

2.3. MPPT Techniques for Multiple Power Peak Curves

Under Partial shading conditions, multiple peaks in the P-V curve and multiple steps in the I-V curve appear. Their presence reduces the effectiveness of MPPT schemes that assume single peak point. Many articles have been proposed for the purpose of developing special schemes to discriminate between local and global peaks without getting stuck at a local one.

Patel and Agarwal [17] propose to use a global peak (GP) track subroutine to scan the P-V curve for the global maximum when a sudden change in power (above a critical value) is noticed. The approach is based on two main assumptions or critical

observations: 1) the minimum voltage displacement between any two, consecutive, local

peaks is nearly 80% of one module's open circuit voltage (V_{oc}), and 2) the magnitudes

of subsequent peaks (whether to the left or right of the GP) continuously decrease. So

with an initial position at a certain local peak, the curve is scanned first to the left of this

peak, by applying voltage perturbation to decrease the operating value, but with

$\Delta V < 80\% * V_{oc}$ so that not to skip a peak. As long as $dP/dV > 0$, continue decreasing V.

Once $dP/dV < 0$, the P&O routine is called and a local peak is tracked. If the new local

power is higher than the old one, it is replaced to be the candidate for the GP, else and

based on their assumption that there are no more peaks of greater magnitude to the left,

the search shifts to the right of the local peak. Similarly, when moving to the right, V is

increased as long as $dP/dV < 0$. Once positive, a new local peak is detected and

compared. If it is found to be less, the right side scanning is stopped and the program

returns the last candidate local peak to be the GP. Raza et al [18] say that this approach

depends on assumptions that cannot be generalized for all conditions and that the

algorithm may fail to track the GP if the P-V curve looks as in [11, Fig. 4], where peaks

do not gradually decrease in magnitude at the left of the GP.

Kobayashi et al [19] use a two-stage approach for global peak detection; the

control strategy in stage 1 aims to move the operating point to the intersection between

the actual multiple step V-I curve and the equivalent load line of slope R_{pm}, which is the

ratio of the optimal voltage to the optimal current under uniform irradiance

($R_{pm} = V_{pm}/I_{pm} = 0.8V_{oc}/0.9I_{sc}$). V_{oc} and I_{sc} are obtained through on-line measurements by

disconnecting the panel from the load every period and short-circuiting it. This

requirement affects the efficiency of the cells and increases the complexity of the

hardware. By this stage, the operating point is assumed to have by-passed all local

maxima and approached the global one. Then in the second step, the IC method is used

to converge to the first maximum reached, supposed to be the global one. Here also

Raza et al [18] state that the assumption of by-passing all local maxima in stage one to

definitely reach the global optimum in stage two cannot be generalized. They show that

more than one peak may lie at the right side of the load line and that the global one may

not be the closest, so the algorithm is trapped at a local peak and fails tracking the GP.

Another two stage method is proposed by Bazzi and Karaki [20] to reach the

global peak. Given the irradiance and temperature measurements of the modules the

overall P-V curve is estimated using standard manufacturer's data and a search

algorithm seeks an approximation of the GP region. This stage does not give the

accurate GP point since it is based on characteristic parameters given by the

manufacturer, which change with time and weather conditions. Then, in step 2, ripple

correlation control (RCC) or a P&O method is executed to accurately converge to the

GP. The method is applicable for a generator of a few modules and cannot handle a

large number of PV panels.

A recent optimization algorithm idea for tracking global maxima is based on

the differential evolution (DE) proposed in [21]. This stochastic population-based

optimization process shows a fast convergence, accuracy in detecting the true GP

whatever initial parameter values were set, and usage of few control parameters. The

approach in general is that certain properties of the system, depending on N_p real-valued

parameter vectors X_i in a population of each generation, need to be optimized. The

optimization is done by varying the D-dimensional vector X_i until the parameters are

optimized. A mutation operation produces a mutant vector for each target vector, being

an individual in the current population, by adding the weighted difference between two

randomly chosen vectors to a third one. Then by mixing the mutant vector with the target in the next crossover operation, a trial vector is generated. If it fits a better optimized objective function than the target vector, it replaces it in the next generation. Else, the parent target vector is retained. Then, for each generation, the best individual is selected.

CHAPTER III

SINGLE PEAK MAXIMUM POWER POINT TRACKING

This chapter presents a novel single peak tracking method. It presents the theory of MPP operation according to this method, the models of the different subsystems used in the simulation, and the implementation details of the PID controller as well as results on the tracking efficiency under various irradiance profiles.

3.1. PV Module: The basic Component

3.1.1. Definition of PV cell

A solar panel is a device which is used to convert energy contained within the sun's rays into electricity. It is made up of a group of solar modules, which are in turn built up from a combination of parallel and series solar cells connected to each other. A solar cell (also called photovoltaic cell) is a solid state electrical device that converts the energy of light directly into electricity by the photovoltaic effect. These cells are made out of a semiconductor, mostly Silicon. Solar energy is in fact delivered in photon packets that hit these solar cells, and are then transformed into electric energy. If the photons are absorbed, and their energy is equal to the band gap energy, which is the amount of energy needed to free an electron from its outermost shell in a Si atom, electron hole pairs are generated. The latter phenomenon is referred to as the photovoltaic effect. These pairs will produce an electric field and thus drive an electric current to flow. The cells must be connected electrically to one another and to the rest of the system. Electrical connections are made in series to achieve a desired output voltage and/or in parallel to provide a desired current capability.
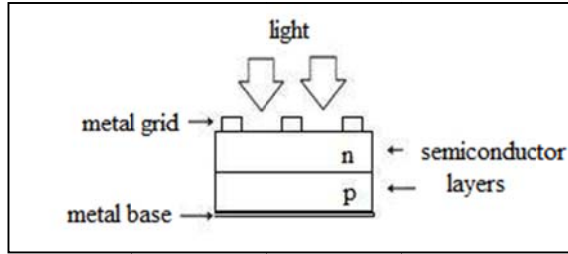
Fig. 1: Structure of a PV cell

3.1.2. Equivalent Circuit of a PV module

The simplest equivalent circuit of a PV module is a current source in anti-parallel with a diode as shown in Figure 2. The output of the current source is directly proportional to the light falling on the cell (photocurrent I_{sc}). During darkness, the solar cell is not an active device; it works as a diode, i.e. a p-n junction. It produces neither a current nor a voltage. However, if it is connected to an external supply (large voltage) it generates a current, called diode current or dark current. The diode determines the I-V characteristics of the cell. The approximation of a capacitor model in parallel with the PV module is necessary as proposed in [4,5] and is considered to be an internal component of the solar module. The per unit area capacitance of a single crystal PV cell at a bias voltage of 0.6 V is approximated to be 1,000 $\mu F/m^2$. The total capacitance for the module consisting of 36 cells in series with each of an area 0.0248 m^2 is 0.69 μF [22].

Fig. 2: Equivalent circuit of a PV module

16

3.1.3. Basic Equations

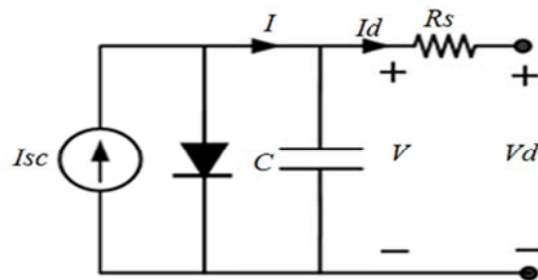The operation of the PV module is described by its characteristic I-V equations, KCL at the capacitor node, and KVL in its output loop. These equations are respectively given by:

$$I = I_{SC} \left(1 - exp\left((V - V_{OC}) / N_S V_t \right)\right) \tag{3.1}$$

$$C \frac{dV}{dt} = I - I_d \tag{3.2}$$

$$V = V_d + I_d R_s \tag{3.3}$$

where V_d is the module terminal voltage, V_{OC} the module open circuit voltage, I_{SC} is the module short circuit current, N_s the number of series cells in a module, V_t the thermal voltage ($V_t = 0.025$V at 300K), I_d the module terminal current, and I the internal current in the module as shown in Figure 2. In practice, I_d and V_d are measured at each sampling time and I is obtained from the non-linear relation in (3.1).

3.1.4. Characteristic Curves of PV modules

Figure 3 shows the power-versus-voltage and the current-versus-voltage nonlinear characteristic curves of a PV module with a single maximum power point lying on the curves of a uniformly shaded array. There is a unique P_{max} corresponding to a voltage V_{pm} and current I_{pm}. The point of coordinates (V_{pm}, I_{pm}) is a point on the load line of slope $R_{pm} = V_{pm} / I_{pm}$. V_{pm} and I_{pm} are approximately equal to 80% and 90% of the open-circuit voltage V_{oc} and short-circuit current I_{sc} of the PV array, respectively. The V_{oc} is the voltage seen at the terminals of the PV panel when no load is connected, and thus zero current flow. The I_{sc} is when the panel voltage is zero, and thus presents the

maximum current a panel can provide. These two parameters mark the intercept values
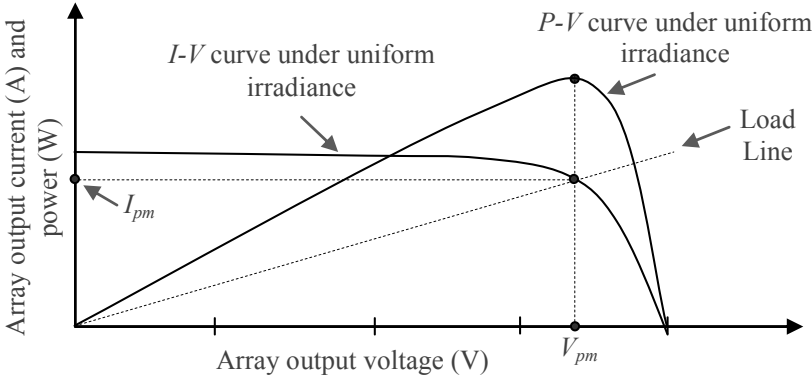
in an I-V or P-V characteristic plot.

Fig. 3: Typical P-V & I-V characteristics of PV modules under uniform irradiance

3.1.5. The Need for tracking the MPP

The MPP tracker is an electronic system that varies the electrical operating

point of the modules so that the modules are able to deliver maximum available power.

MPPT is not a mechanical tracking system that physically moves the modules to make

them point more directly at the sun. In general, the MPPT algorithm works in

conjunction with a dc–dc power converter, whose duty cycle is modulated in order to

track the instantaneous MPP of the PV source. A controller is used to implement the

proposed MPPT algorithm and give a pulse width modulation (PWM) to drive the boost

DC/DC converter and force the PV module to operate at the MPP.

The characteristic curves specify a unique operating point at which maximum

possible power is delivered. At the MPP, the PV operates at its highest efficiency. The

amount of power generated by a PV depends on the operating voltage of the array, thus

the need to set the PV array at an operating voltage corresponding to the MPP. Under

uniform solar insolation, the P–V curve of a PV module exhibits only one MPP for a given temperature and insolation. The matter is further complicated due to the dependence of these characteristics on the operating temperature and on the level of irradiance. The latter two effects can influence the open circuit voltage (V_{oc}) and the short circuit current (I_{sc}), which are important parameters that shape the characteristic curves and thus the MPP. Temperature and solar irradiance are capable of changing these two parameters. As these parameters vary continuously, the MPP also varies, thus the need to keep tracking it as conditions change. Considering the high initial capital cost of a PV source and its low energy conversion efficiency, it is imperative to keep operating the PV source at the MPP and to keep tracking this electrical operating point so that maximum power can be extracted.

A change in temperature will affect the open circuit voltage more heavily than short circuit current of the panel, and the opposite is true for irradiance changes. In fact, as irradiance S increases, I_{sc} increases but V_{oc} slightly changes. However as temperature T increases, V_{oc} decreases but I_{sc} slightly changes. Figure 4 shows the effect of varying irradiance and how the MPP changes as weather conditions change. Consider that curve (a) is for solar irradiance of 80% sun (800 W/m²). When the irradiance is at 40% sun, then the short circuit current drops by 50%, whereas the open circuit voltage drops by about 3% for a module with 36 series cells. So the new I-V characteristics are approximately as shown in Figure 4, curve (b). Point P_1 is the MPP at 80% sun. At 40% sun, the operation shifts to a new intermediate point P_2. The voltage at P_2 is the same as at P_1 since the duty cycle has not changed. The MPPT controller will then, through one of the MPPT algorithms change the duty cycle D of the converter and change operation to P_3, the new maximum at the new irradiance level.
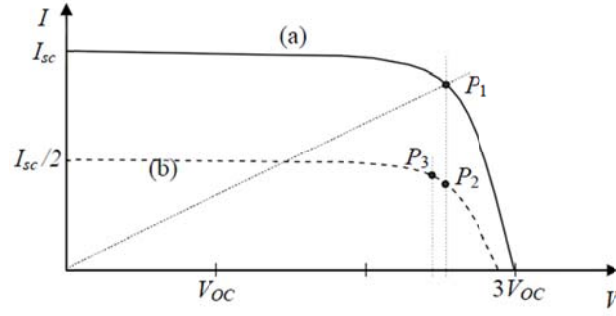
Fig. 4: Maximum power points at 80% sun (P_1) and 40% sun (P_3)

3.2. Dynamic Model of PV-Converter System

The system is composed of a PV module charging a battery via a DC-DC boost converter and a MPPT controller, as shown in Figure 5.
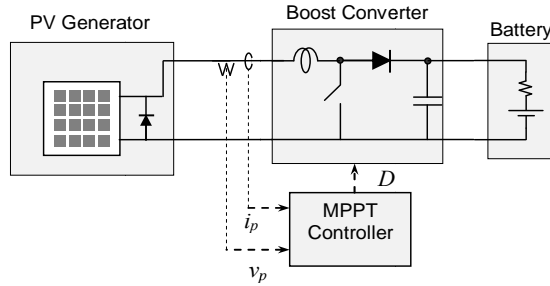
Fig. 5: System model of a PV module charging a battery via a boost converter with an MPPT algorithm implemented.

The problem is explained using a battery as the load. In many cases, the boost converter will be feeding a DC-AC switching inverter being connected to the grid. So the model may also represent a single phase grid connection, which would have a constant voltage reflection (V_b) on the boost converter output given by [22]:

$$V_b = \frac{\sqrt{2} * V_{g1}}{m_a} \tag{3.4}$$

where m_a is the amplitude modulation index usually equal to 1, and V_{g1} is the fundamental of the grid line-neutral rms voltage.

The anti-parallel diode is used in case more than one module is operating in series, to protect the circuit from current conduction limitations that might arise in case of partial shading. The operation of the boost converter (Figure 6) is described by KVL of the input loop and KCL at the capacitor node which in differential form are given by:

$$V_d = L\frac{dI_d}{dt} + I_d R_L + V_0(1 - S) \tag{3.5}$$

$$C_0\frac{dV_0}{dt} = I_d(1 - S) - (V_0 - V_B)/R_B \tag{3.6}$$

where V_0 and C_0 are the output capacitance and voltage across it, and V_B and R_B are the battery voltage and internal resistance. Note that the current in the inductance is equal to the output current of the PV module, I_d. The variable S represents the switch status, which is equal to 1 when the switch is on and 0 when it is off. The state of the switch at each sampling time is determined by a pulse width modulation technique that compares the duty ratio value with a triangular signal going from 0 to 1 each time period T_s. When D is greater than the triangular signal value, the switch is set to one; else it is set to zero. The duty cycle is given by $D = T_{on}/T_s$ with D varying between 0 and 0.75. The boost converter's relationship between its input and output voltages is given by [23]:
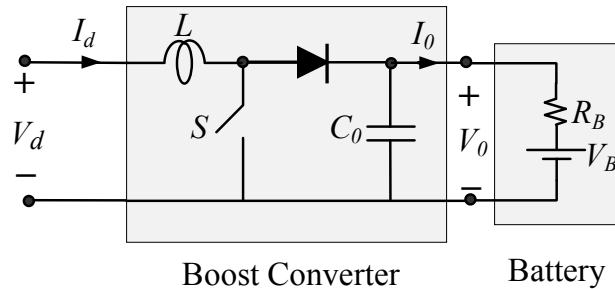
$$V_d = V_0 (1-D) \tag{3.7}$$

Fig. 6: Boost converter and battery circuit diagram

3.3. Dynamic Solution of PV-Converter Model

The system model is based on solving the algebraic-differential system of equations (3.1), (3.2), (3.3), (3.5), and (3.6) using the implicit trapezoidal (IT) method, which is widely used in power system transient analysis due to its excellent stability and good accuracy [24]. For convenience the IT method is illustrated using the following first order DE:

$$\frac{df(t)}{dt} = y(t) \tag{3.8}$$

Given the solution at time t as $f(t)$, then the solution at time step $t + h$ by the IT method is given as:

$$f(t + h) = f(t) + \frac{h\,(y(t) + y(t+h))}{2} \tag{3.9}$$

At time $t + h$ the value $y(t + h)$, which in general is a function of $f(t)$ is not initially available and has to be estimated by $y(t)$. Once $f(t + h)$ is calculated a new value for $y(t + h)$ is determined and the iterative process taking place over one time step is repeated a number of times until two successive values of $y(t + h)$ are sufficiently close.

Equations (3.2), (3.5), and (3.6) are put in the IT form respectively as follows:

$$V(t + h) = V(t) + \frac{h\,(I(t) + I(t+h) - I_d(t) - I_d(t+h))}{2C} \tag{3.10}$$

$$I_d(t + h) = I_d(t) + \frac{h\,(V_d(t) + V_d(t+h) - (V_0(t) + V_0(t+h))(1-S))}{2L} \tag{3.11}$$

$$V_0(t + h) = V_0(t) + \frac{h\,(2V_B - V_0(t) - V_0(t+h) + (I_d(t) + I_d(t+h))(1-S)R_B)}{2C_0 R_B} \tag{3.12}$$

In the above equations $I(t)$ is evaluated using (3.1) with V replaced by its value given by (3.3).

3.4. MPPT Controller

The continuous switching operation causes natural ripples in the voltage and current waveforms of the PV module as shown in Figure 7. Note the narrow variation in the voltage compared to the relative wide variation in the current as implied by the form of the I-V curve in the neighborhood of Point 1.The relationship between the magnitudes of the voltage and current ripples changes as the operating point shifts from Point 1 to Point 2 (Figure 8). These ripples may be used to define an incremental conductance; for example at Point 1:

$$\Delta I_1/\Delta V_1 = (I_{1b} - I_{1a})/(V_{1b} - V_{1a}) \tag{3.13}$$

The incremental conductance at point 2 is similarly defined and has a value much lower than that of Point 1. To move from Point 1 to the MPP, we need to reduce the PV module voltage V_d as given by (3.7), so D should be increased. Similar analysis for the operating Point 2 implies that we need to increase the voltage V_d and thus reduce the duty cycle D.

The required change in the duty cycle is obtained using a digital proportional-integral-derivative (PID) controller that aims to equalize the average and incremental inductances as explained below. The duty ratio is varied by the MPPT controller according to the error away from the MPP. This would vary the operating voltage V_d of the panel as V_0 is a constant load voltage.
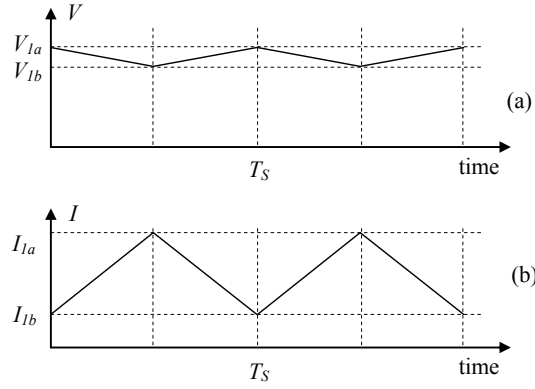
Fig. 7: Waveforms of voltage (a) and current (b) at Point 1
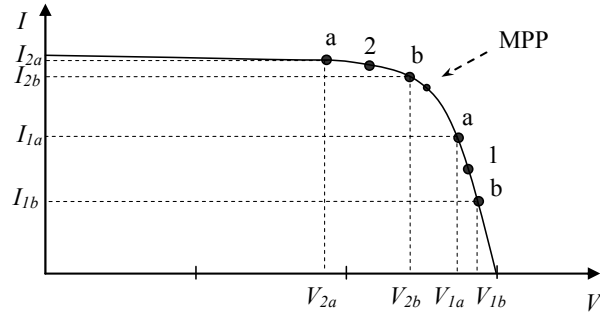
Fig. 8: Voltage and current variation at operating points P_1 and P_2

3.4.1. Methodology

At the maximum power point (MPP), the slope dP/dV of the power versus voltage curve is 0, thus:

$$d(VI)/dV = V\, dI/dV + I = 0 \qquad (3.14)$$

which implies that at the MPP, the incremental slope is the negative of the average conductance of the module. This may be conveniently written as an error signal e that should be equal to zero at the MPP:

$$e = \left| \Delta I / \Delta V \right| - I/V = 0 \qquad (3.15)$$

24

During operation, the controller block shown in Figure 5 samples the voltage of the module and the current fed out into the inductor at the time of switching. The sampled values represent a maximum or a minimum. After taking several samples for each of the voltage and the current, the incremental and average conductance can be calculated. Their difference is the error e input of the PID controller. Note that in (3.15) the magnitude of the incremental slope $\Delta I/\Delta V$ can be approximated from the ratio of voltage and current swings. And the average values of the signals provide the values for V and I. The error e at points other than the MPP is not zero and is used as input to the PID controller with zero reference. For instance, at Point 1 in Figure 8, to the right of the MPP, the error $e > 0$ and the PID controller acts to reduce the voltage of the PV generator voltage by increasing the duty ratio of the boost converter.

3.4.2. PID Controller Tuning

The main function of the PID controller is to bring the offset error e, as evaluated from the voltage and current ripples using (3.15), to zero. According to the error feedback, the controller applies a combination of proportional, integral, and derivative control to appropriately modify the duty cycle of the boost switch using the following well known formula:

$$\Delta D = K_p e + K_i \int_0^t e\, dt + K_d\, de/dt \tag{3.16}$$

The integral term is evaluated incrementally at each sampling time interval as the sum of the error at the previous sampling interval plus the integral of the error over the last sampling time interval evaluated using the trapezoidal rule. The error sampling skips two cycles after each measurement, so that the system's behavior settles down. So

the time difference separating the two error samples is $2T_s$. The integral term is calculated as follows:

$$\int_0^t e\, dt = \int_0^{t-1} e\, dt \; + \; 2T_s(e(t) + e(t-1))/2 \tag{3.17}$$

The derivative term finds the rate of error change between two samples, and is evaluated as follows:

$$de/dt = \; (e(t) - e(t-1))/2T_s \tag{3.18}$$

An initial value of the constant K_p is obtained by consideration of the maximum possible error when the operating point is at extreme point at the open circuit voltage (V_{oc}), with K_i and K_d set to zero. So K_{pmax} is then given by:

$$K_{pmax} = \; \Delta D_{max}/\Delta e_{max} \tag{3.19}$$

with

$$\Delta e_{max} \cong \Delta I_{max}/\, \Delta V_{max} \; = \; I_{MPP}/(V_{oc} - V_{MPP}) \tag{3.20}$$

$$\Delta D_{max} \; = \; (V_{oc} - V_{MPP})/\, V_0 \tag{3.21}$$

where I_{MPP} ($\cong 0.93 I_{sc}$) and V_{MPP} ($\cong 0.75 V_{oc}$) are the current and voltage values at the maximum power point, which are normally given by the manufacturer at standard conditions. The terms K_p, K_i, and K_d are chosen by manual tuning as proportions of $K_{pmax} \cong 0.15$.

3.5. Simulation Results

The system being simulated consisted of an ISTAR 135 PV module with $V_{oc} =$ 21.8 V and $I_{sc} = 8.3$ A at standard conditions. The module has 36 series cells with a total area of 0.893 m^2, an estimated series resistance of $R_s = 0.249\ \Omega$, and a junction

capacitance of 0.69×10^{-6} F. The ambient temperature was fixed at 30°C. The boost

converter has an input inductor with $L= 2.5 \times 10^{-3}$ H and $R_L= 0.12$ Ω. The voltage across

the switching device was taken to be 0.36V and the voltage drop in the diode was taken

to be 0.8V. The battery voltage is 24V and its internal resistance is 0.04 Ω. The

switching frequency of the boost converter was 25 kHz.

A simulation test was carried out at various irradiance levels to monitor the

behavior of the system and study the tracking and the overall system efficiencies.

Irradiance level steps of 400, 800, 1000, 600, and 400 W/m^2 are successively applied

during different intervals for a study period of 20 ms. The results are shown in Figures

9 through 14. The controller succeeds to set the PV generator's output power at the

maximum power point at each level, even under sudden rapidly changing conditions.

The results also demonstrate the natural steady state ripples in the voltage and current

signals.

27
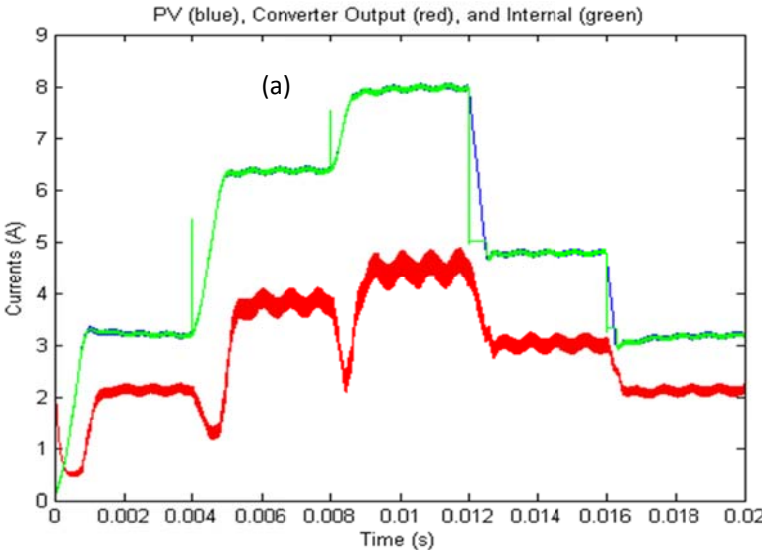
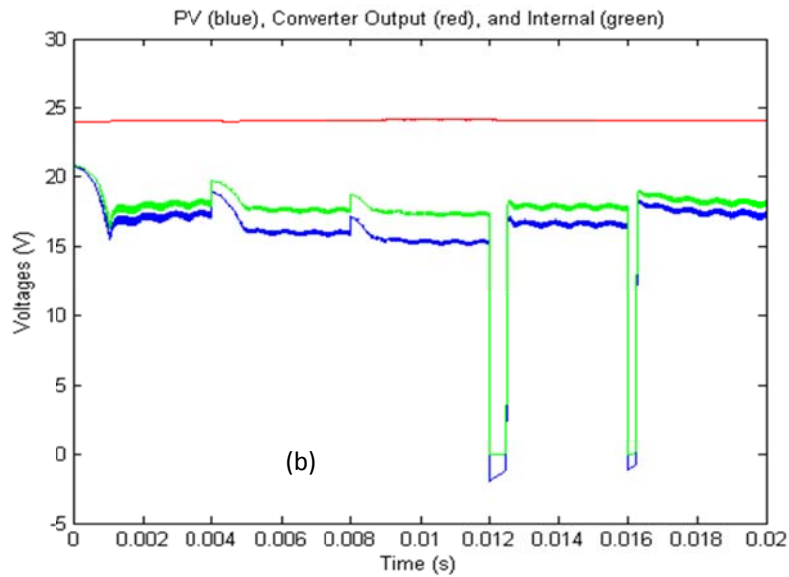Fig. 9: Simulation results: (a) current and (b) voltages.

The power curves for the same simulation trial are shown in Figure 10. It is noted that when the solar irradiance is abruptly decreased, the voltage of the PV panel may momentarily drop to zero because of the current at the previous larger irradiance level that may be greater than the new short circuit current.
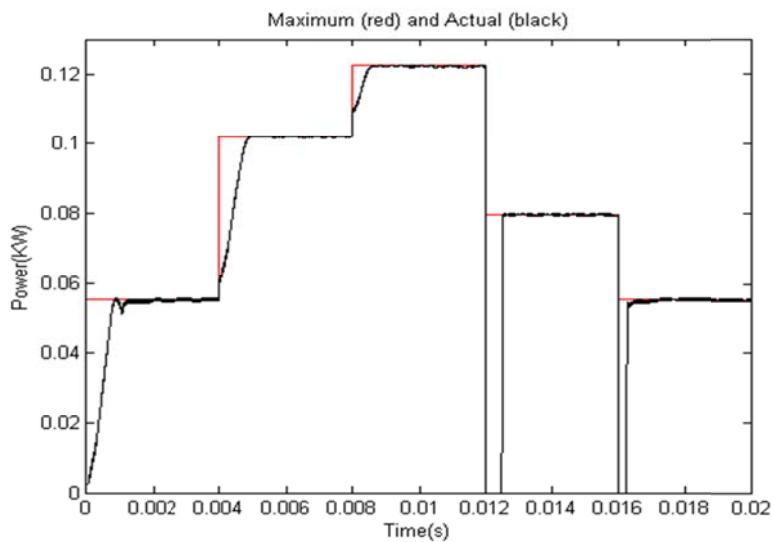

Fig.10: Simulation results: power curves

The voltage recovery occurs when the inductor current drops below the short circuit current. During this time, the system is kept idle for it to stabilize, without any tracking control taking place and the duty cycle kept at its current value. This phenomenon also appears in the voltage curves in Figure 9 (b) at the fourth and fifth irradiance step changes.

The efficiency of the system was monitored during this simulation test and a summary of the system and tracking efficiency is given in Table 1. The tracking efficiency given in equation (3.22) is the ratio of the actual power to the maximum possible power at the current irradiance level, i.e. it is the ratio between the power curves in Figure 10. During the transient following a change of irradiance, the efficiency somewhat drops but recovers very quickly to a high value of about 99.85% or higher. The efficiency of the boost converter (3.24) is in the region of 90%. Note that the PV module efficiency (3.23) drops at high irradiance levels because its operating temperature rises and more heat is lost to the ambient. The overall efficiency (3.25) figures shown are typical of a mono-crystalline PV module.

$$efficiency\ of\ tracking(\%) = \frac{P_{actual}}{P_{max}} \times 100 \tag{3.22}$$

$$PV\ module\ efficiency = \frac{P_{max}}{G*A_{cell}*N_S} \times 100 \tag{3.23}$$

$$Converter\ efficiency = \frac{V_0*I_0}{V_d*I_d} \times 100 \tag{3.24}$$

$$overall\ efficiency = \frac{P_{max}}{G*A_{cell}*N_S} \times \frac{P_{actual}}{P_{max}} \times 100 = PV\ eff * tracking\ eff \tag{3.25}$$

Table 1: Components and Overall System Efficiencies in Percent

	400 W/m^2	800 W/m^2	1,000 W/m^2	600 W/m^2	400 W/m^2
Tracking	99.60	99.90	99.85	99.88	99.89
PV module	15.8	14.6	14.0	15.2	15.8
Converter	93.6	90.4	88.8	91.7	93.0
Overall	14.8	13.2	12.4	13.9	14.7

The step length selected for the IT method has to be smaller than the correction coefficient associated with the different equations (i.e. $h/2C$, $h/2L$, and $h/2C_0$). When $h = T_s/50 = 8 \times 10^{-7}$, these coefficients have the following values respectively 0.58, 1.6× 10^{-4}, and 1×10^{-4}. Clearly the system is stiff, and the first value is inappropriately large and would lead to convergence difficulties. The value of $h = T_s/250 = 1.6 \times 10^{-7}$ gives coefficient values of 0.116, 0.32×10^{-4}, and 0.2×10^{-4}, which were found to work appropriately. The solution time it took to simulate the system over a simulation of $500 T_s = 20 \times 10^{-3}$ s was 24.3 seconds.

The tuning of the PID controller started from the value of $K_p = 0.6 K_{pmax} = 0.09$, then appropriate values of K_d and K_i were found by trial and error. Neither the first Ziegler-Nicholson rule nor the second rule was noted to be applicable in this case.

The duty cycle variation during the simulation trial is shown in Figure 11 and the errors are shown in Figure 12 above. For proper operation, the error limiter was included in the controller to limit the error value to a maximum of ±1and the duty cycle was also limited to a range of 0 and 0.75. Operation above 0.75 is not possible due to the effect of parasitic elements [23].
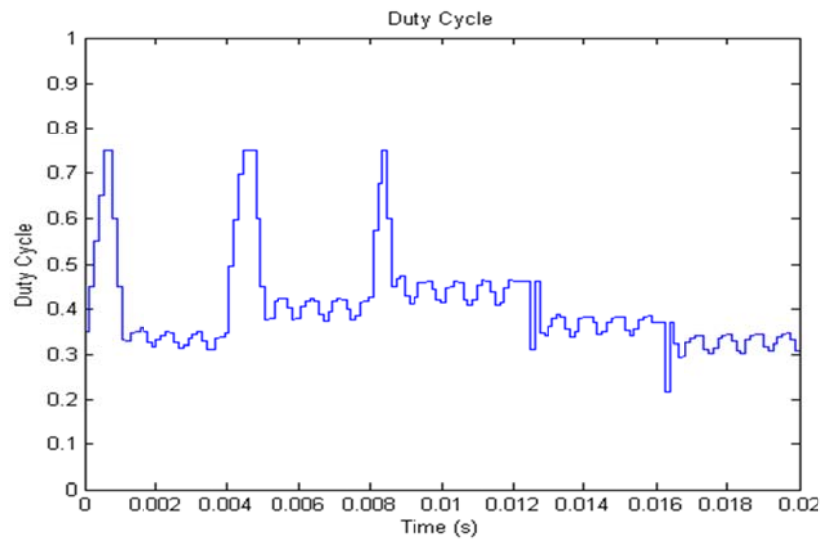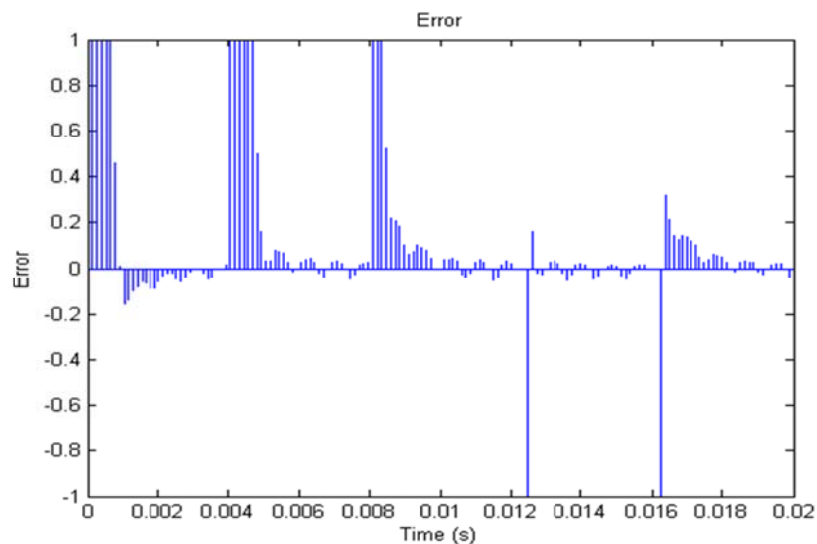
Fig.11: Simulation results: duty cycle

Fig. 12: Simulation results: tracking error

The natural inherent current and voltage ripples during the simulation trial are shown above in Figures 13 and 14 respectively. The phenomenon of natural ripples in the voltage and current waveforms of the PV module due to continuous switching operation was explained theoretically in Figure 7 previously and is shown here by simulation. Note the opposite slopes of variation between the current and the voltage as implied by the form of the I-V curve, in which current increases as voltage decreases

and the opposite. Also, note the shift between the module terminal current and the internal current in the module due to the internal capacitance component in the PV module.
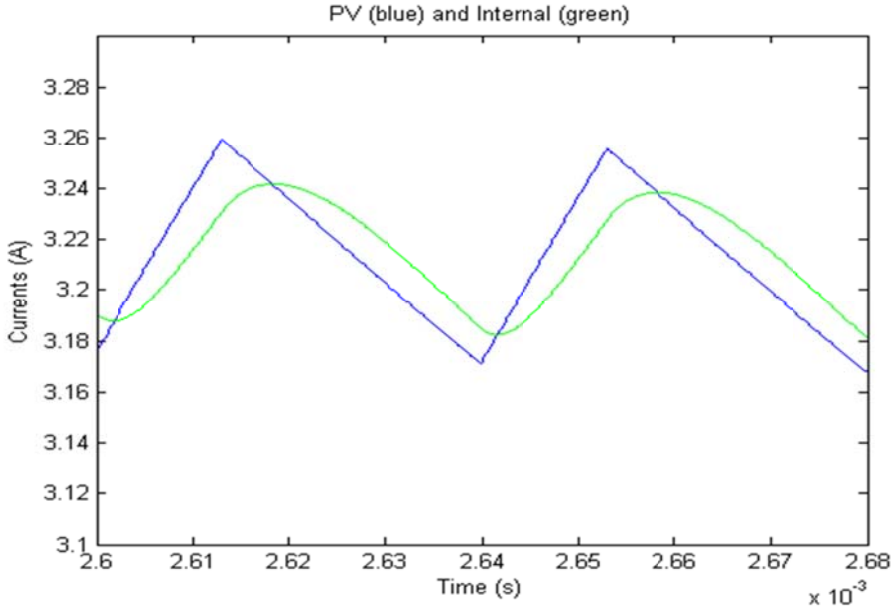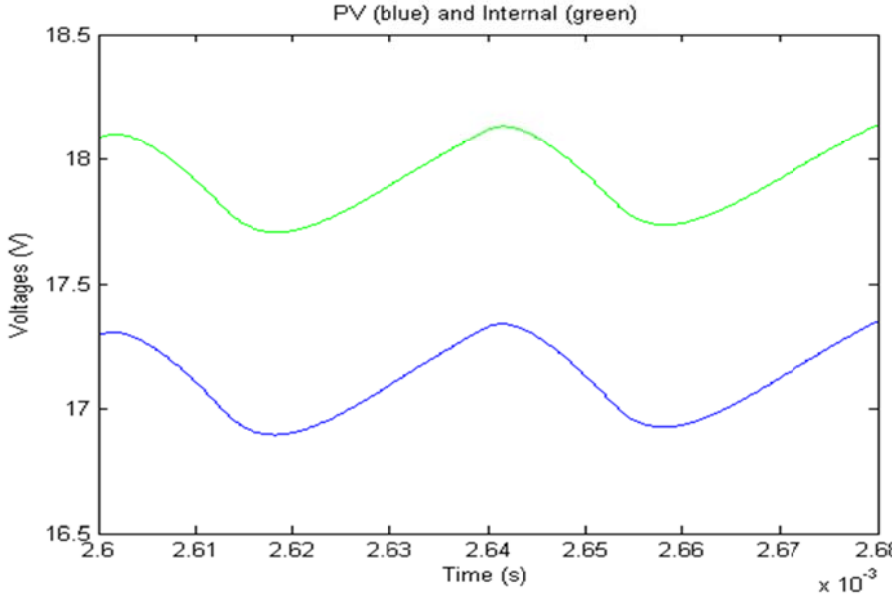

Fig.13: Simulation results: Current Ripples

Fig.14: Simulation results: Voltage Ripples

CHAPTER IV

MODELING OF PARTIALLY SHADED PV PANELS

The aim in this chapter is to model a PV array taking into account the temperature, sun's irradiance, and partial shading factors, to determine its current-voltage and power-voltage characteristics. This enables the dynamics of PV system to be easily simulated and later optimized. The chapter will present a MATLAB-based modeling and simulation scheme suitable for studying the I–V and P–V characteristics curves of a PV array with partial shading configuration given the exact irradiance values.

4.1. Components of PV Array

It is not only the size (i.e., the total number of modules) of the PV array but also its configuration (i.e., the number of modules in series and parallel) that significantly affects its power output. Thus, the performance of the system is generally affected by temperature, solar irradiance, shading, as well as array configuration. Under partially shaded conditions, the PV characteristics get more complex with multiple peaks. So it is important to show how PV modules are further classified according to different shading levels forming an overall array configuration.

A special categorization and terminology is used to describe the various components of a PV array. The basic elementary component of a PV array is the PV cell, characterized by its V_{oc} and I_{sc} specified in its data sheet. In our study, the PV module considered consists of 36 PV cells connected in series providing an open circuit voltage of 21.8 V and a short-circuit current of 8.3 A. In Figure 15, each module has a

bypass diode in parallel with it, omitted from the diagram to simplify the drawing. The gray color indicates that a module is partially shaded and the white color implies that it is un-shaded. A subassembly (such as S_1 or S_2) is formed of several series-connected PV modules receiving the same level of irradiance. Several series connected subassemblies, each with a different irradiance level, form a full series assembly (S_1 in series with S_2). Series assemblies, having similar shading patterns, form a group (such as G_1 or G_2). Various groups (with the ith group represented by G_i), having different shading patterns and connected in parallel, form the PV array. The series blocking diodes prevent the flow of reverse current into assemblies with lower irradiance, which generate a lower output voltage thus causing excessive heat generation and thermal breakdown [6].
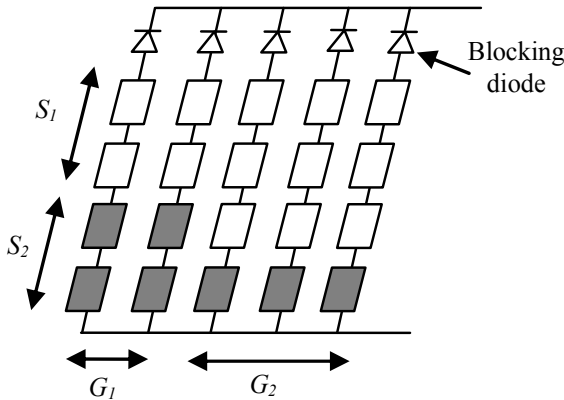

Fig. 15: PV array components.

4.2. Modeling Methodology

Two cases will be illustrated for getting the characteristic curves. The first is the case of two or more modules in series subjected to different irradiance levels. The second is the case of two or more series-assemblies in parallel forming different shading patterns.

34

4.2.1. Combining Series Modules

The methodology of combining series modules to determine their I-V and P-V curves is explained using a simple example of two modules in series having different irradiances as shown in Figure 16. Across each module is a bypass diode to protect the circuit from current conduction limitations that might arise in case of partial shading. Fig. 16 (a) shows two modules connected in series each under a different irradiance level value Gi in W/m2 and assuming G1 > G2. The corresponding I-V curves of the two modules are represented in Fig. 16 (b) showing different short circuit currents Isc1 and Isc2 with Isc1 > Isc2 since module 1 is exposed to a larger irradiance value than module 2.
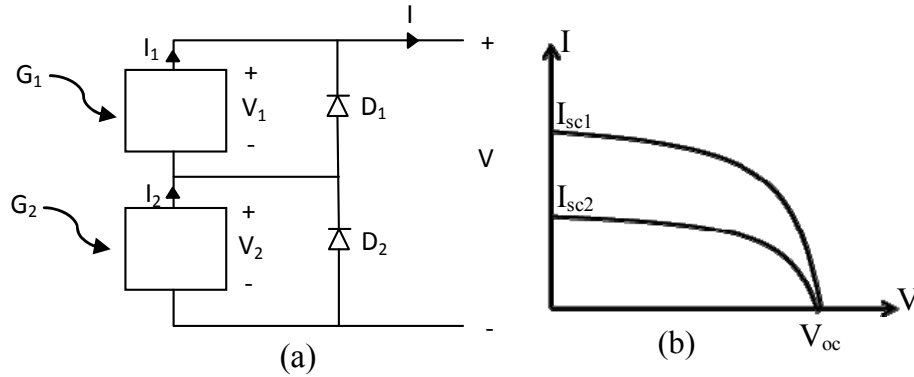

Fig. 16: Two series connected modules under different irradiance levels (a), I-V curves of the two modules (b).

The overall I-V curve of the two modules in series is obtained by varying the current I from $I_{max}=$ max (I_{sc1}, I_{sc2}) down to zero in steps of ΔI (e.g. $0.001* I_{max}$) and such that for each value I:

$$\text{If } I > I_{sc2}, V = V_1 - 0.7 \text{ }, (D_2 \text{ is on}, D_1 \text{ is off}) \tag{4.1}$$

$$\text{If } I < I_{sc2}, V = V_1 + V_2 \text{ }, (D_1 \text{ and } D_2 \text{ are off}) \tag{4.2}$$

$$\text{With: } V_i = V_{oci} + N_{si}V_t \ln\left(1 - \frac{I}{I_{sci}}\right) - IR_{si} \tag{4.3}$$

and V_i may be V_1 or V_2.

In general when several modules are in series and $I > Isci$, module i is bypassed by its corresponding diode considered to be shaded, thus acting as a load consuming a power of $0.7*I$. However, when $I < Isci$, module i will be generating power to the load equal to V_i*I with the voltage across it is calculated according to (4.3).

The function *PVpanel* is the function called by the main program to get the characteristic curves of each series assemblies. It takes as parameters an array of the temperature and irradiance values of all the modules in the series assembly and the number of the modules in series in that assembly. It returns the vectors of output current, voltage, and power values across the total series assembly. The curves are then plotted in the main.

4.2.2. Combining Parallel Strings of Series Module

When different series-assemblies are in parallel as shown in Figure 17 (a), the I-V curves of each series assembly alone is obtained using the procedure outlined above and are as shown in Figure 17 (b). In pattern 1 there is a uniform irradiance so the I-V curve (in blue) shows a single peak. Two different irradiance levels appear in pattern 2; thus its I-V curve (in red) shows 2 peaks. In pattern 3, three different levels of irradiance appear thus causing 3 peaks in the I-V curve (in green).

The approach for computing the I-V characteristics of an array consisting of parallel connected series-assemblies is as follows:

1) Find the maximum open-circuit voltage V_{oc} among all the different series-assemblies.

2) Start varying the voltage V from the maximum value down to zero in steps of ΔV.

3) At each value V, find the corresponding I_i of each series-assembly i from a look up table that is obtained for each series-assembly as explained above (section 4.2.1). If $V_i > V_{OC}$ for assembly i, then I_i is set to zero.

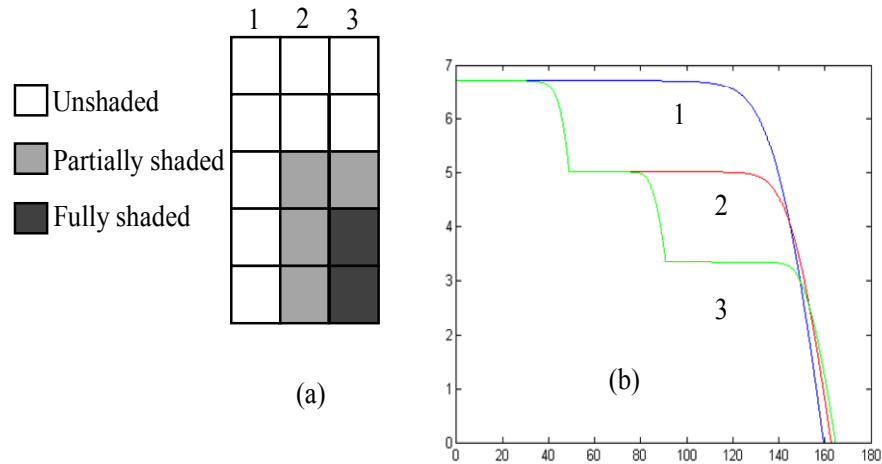4) Add the currents I_i. Decrement V and repeat Step 3.

Fig. 17: Representation of three series-assemblies in parallel (a),
I-V curves for each series-assembly (b).

4.2.3. Overall Algorithm

Figure 18 below is a flowchart summary of the algorithm described in the above two sections. The following is a brief explanation for each block in the flowchart:

1) Step 1: The following symbols (defined as below) are identified by the user:

- $G\rightarrow$ number of groups of identical solar radiation distribution.

- $S\rightarrow$ number of series rows in the PV array.

- $P\rightarrow$ number of parallel columns in the PV array.

- $m(G)\rightarrow$ a row of G columns (the column value $m(i)$ defines the number of series assemblies in group i)

37

- *irradiance(G,S)*→ an array of *G* rows and *S* columns. Each row *i* (where *i* donates the group number and varies from 1 to *G*) is an array of the irradiance values of each of the *S* modules in a series assembly of group *i*.

- *temperature(G,S)*→ an array of *G* rows and *S* columns. Each row *i* (where *i* donates the group number and varies from 1 to *G*) is an array of the temperature values of each of the *S* modules in a series assembly of group *i*.

2) Step 2: For each group *i*, the subroutine *PVpanel* is called to determine the I-V and P-V characteristics of a series assembly of group *i*. It takes as arguments the variable S and the arrays of irradiance and temperature values of the modules in that series-assembly *irradiance(i,:)* and *temperature(i,:)*.

3) Step 3: For each module *j* (where *j* donates the module number in the series assembly and varies from 1 to *S*), the following are calculated: the cell temperature $T_c(j)$, the module open-circuit voltage $V_{oc}(j)$, and the module short-circuit current $I_{sc}(j)$.

4) Step 4: In a for loop, a variable I_s is each time incremented by ΔI=0.001 starting from zero as an initial value to end up at a value equal to the maximum short circuit current $I_{sc}(j)$ among the *S* modules.

5) Step 5: At each value I_s, module *j* whose $I_{sc}(j)$ is more than I_s is considered un shaded and the voltage across it $V_m(j)$ is calculated based on equation (4.3) and module *j* whose $I_{sc}(j)$ is less than I_s is considered shaded and the voltage across it $V_m(j)$ is –0.7 V.

6) Step 6: At each value I_s, voltages $V_m(j)$ are summed up for all *j* from 1 to *S*. $\sum_{j=1}^{S} Vm(j)$ is the value of the voltage *V* across the series-assembly at a current $I = I_s$. The set of values *V* and *I* for all values samples I_s form an array V_t and I_t.

7) Step 7: Having an array V_t for each series assembly of group i, set $V_{max} =$

max(max(Vt)) for all i from 1 to G.

8) Step 8: In a for loop, a variable V_s is each time decremented by $\Delta V = 0.001$ starting

from a value equal to the maximum open circuit voltage among the G series assemblies

till zero as a final value.

9) Step 9: For a series assembly of every group G, interpolate (V_t, I_t, V_s) to get the value

I_i corresponding to V_s for that series assembly. If V_s is more than V_{OC} for that assembly,

I_i is set to zero.

10) Step 10: Add the currents I_i. Decrement V_s and repeat the previous step until it
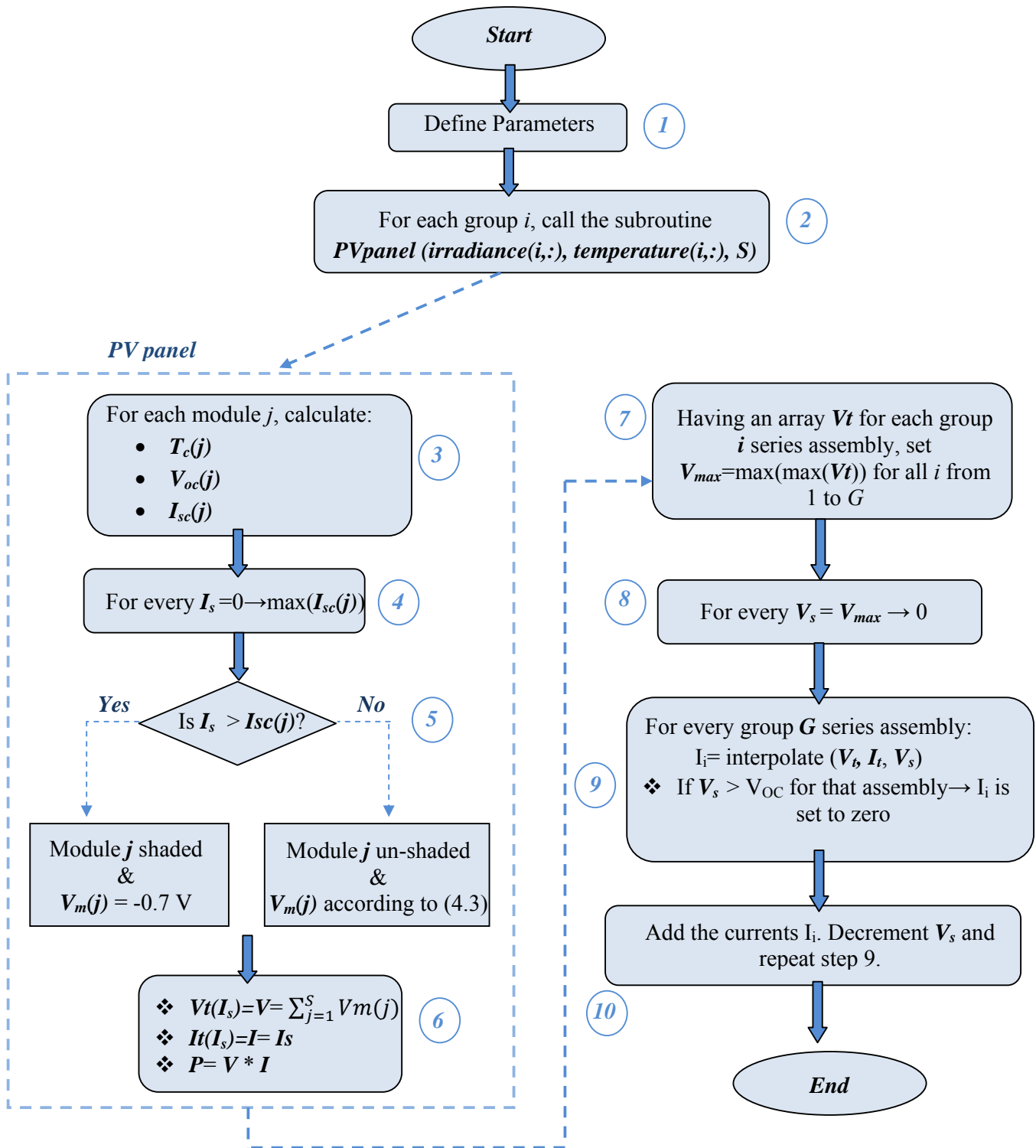
reaches zero.

Fig. 18: Overall algorithm flowchart for determining the characteristic curves.

4.3. Simulation Results

Figure 19 shows a PV array consisting of 10 modules in series and with 10 such series-assemblies in parallel. The different shading patterns define 3 types of series-assemblies and thus 3 groups. Group 1 has uniform irradiance and is formed of 3 series-assemblies, group 2 has 2 different irradiance levels and is formed of 3 assemblies, and group 3 has 3 irradiance levels of 4 assemblies. The I-V curves of each series assembly are obtained as an array of points by adding voltages in the series procedure above (section 4.2.1), and then these curves are combined by adding the currents at the sampled voltages, by using the parallel procedure, as explained above (section 4.2.2).
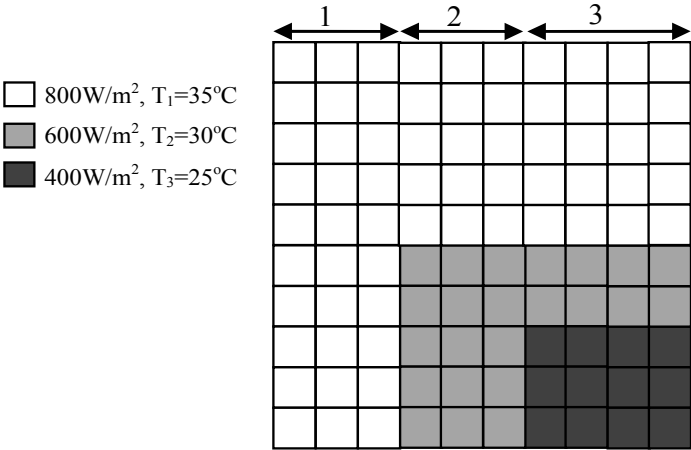

Fig. 19: An array of 10×10 modules at 3 different irradiance levels.

Figure 20 shows the I-V and P-V curves for a series-assembly from each group. For assemblies of Group 1, the curves are similar to a typical PV module because the conditions are uniform on all the modules in the group. Those from Group 2 show two peaks due to the two different irradiance levels. Three peaks appear in the characteristics of the assemblies from Group 3 where three irradiance levels occur. The

I-V and P-V curves of the array under the shown non uniform irradiance pattern are obtained in Figure 21.
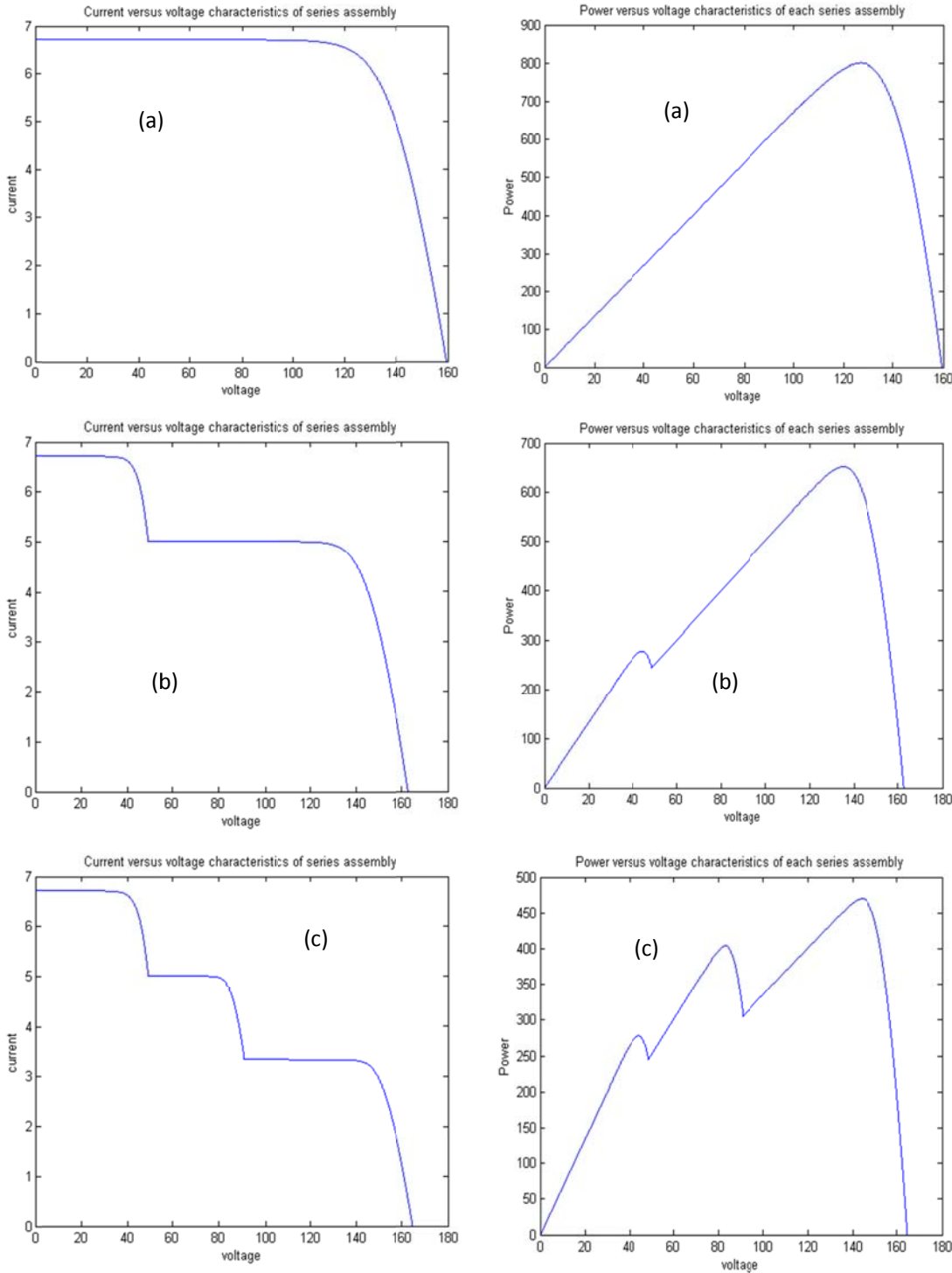

Fig. 20: The I-V and P-V curves of series-assemblies. (a) Group 1. (b) Group 2. (c) Group 3
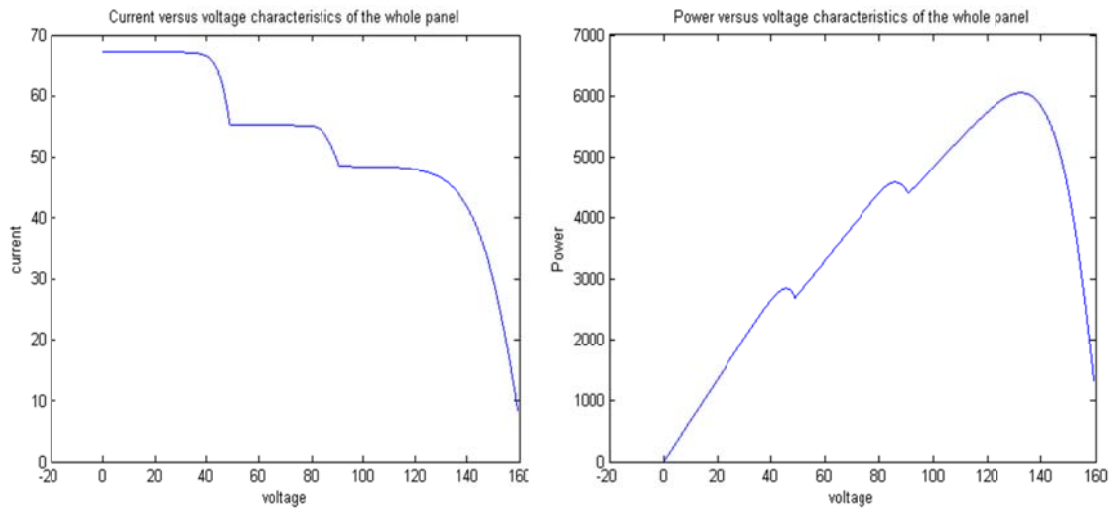
Fig. 21: The I-V & P-V curves of the 10*10 array

Two (10*10) arrays, one for irradiance values and the other for temperatures, are to be assumed defined. For each column (representing a series assembly), the algorithm explained in section 4.2.1 is run and Figure 20 is obtained. The 10 previously obtained series assemblies are now connected in parallel and the algorithm explained in section 4.2.2 is run for obtaining the behavior of the whole panel shown in Figure 21.

4.4. Critical Observations

4.4.1. Observation One

Figure 22 shows a PV array consisting of 10 modules in series and with 10 such series-assemblies in parallel. The scenario assumes that that a 400 W/m^2 shading pattern, covering 4*4 modules of the panel, is gradually moving along the diagonal. This can possibly happen due to a passing by cloud. Each shading pattern position defines 2 types of series-assemblies and thus 2 groups. Group 1 has uniform irradiance and is formed of 6 series-assemblies. Group 2 has 2 different irradiance levels, in which 4 modules in series are shaded and 6 modules in series are un-shaded, and is formed of

4 assemblies. Four gradual moving positions are considered. The objective is to determine the characteristic curves in each shading position for comparison and to deduce if the position of the same shading pattern affects the performance of the PV panel or not.
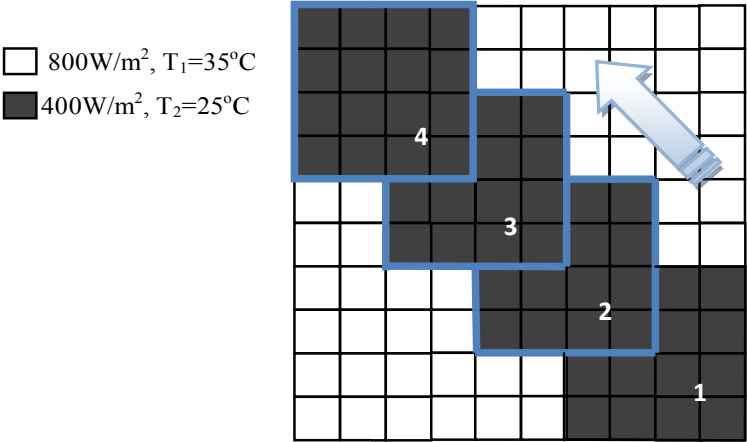

Fig. 22: An array of 10×10 modules at 4 successive moving positions of the same shading. (Observation 1 scenario)
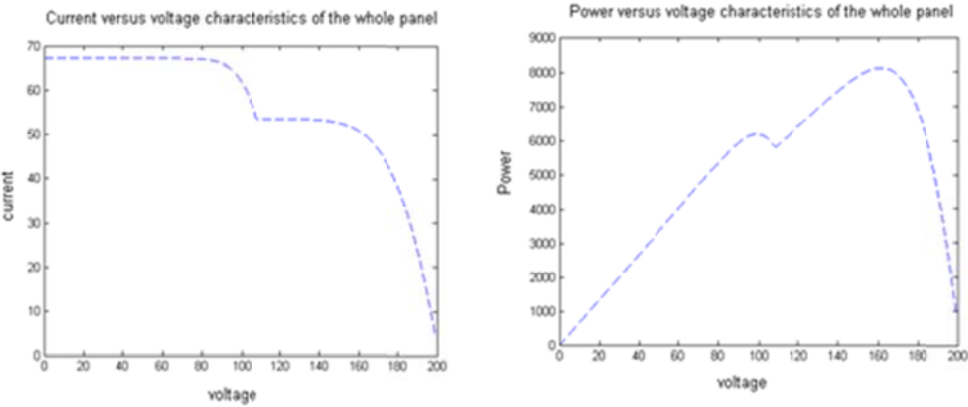

Fig. 23: The I-V & P-V curves of the 10*10 array at each moving position: 1, 2, 3, and 4 of same shading irradiance levels. (Observation 1 scenario)

Figure 23 above shows the obtained I-V and P-V curves for each shading position. The curves for the 4 shading position cases coincide. It is deduced that the behavior is the same no matter where the shading pattern is located on the panel, as long as the shading pattern itself remained the same regarding the irradiance level and the number of modules covered.

4.4.2. Observation Two

Figure 24 shows a PV array consisting of 10 modules in series and with 10 such series-assemblies in parallel. The scenario is similar to that in observation one except that the irradiance level of shading is not kept the same. It is gradually decreasing, as the shading pattern is moving along the diagonal, from 700 W/m^2 in position 1 to 400 W/m^2 in position 4. In other words, the level of shading increased (i.e. the level of irradiance decreased) as the shading pattern moved from position 1 to 4.
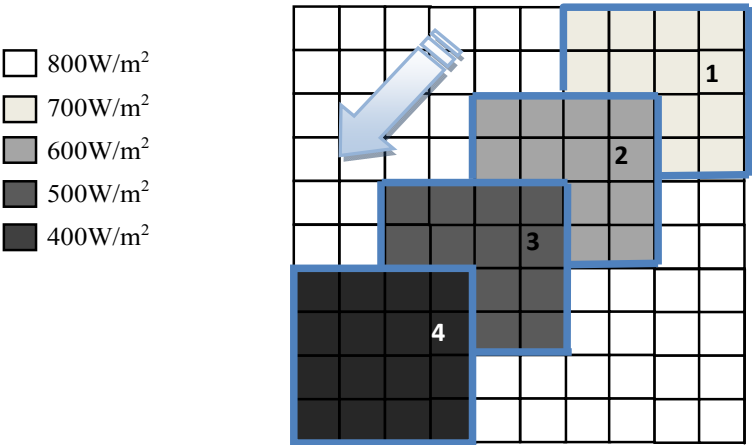

Fig. 24: An array of 10×10 modules at 4 successive moving positions of different shadings (Observation 2 scenario-diagonal movement)
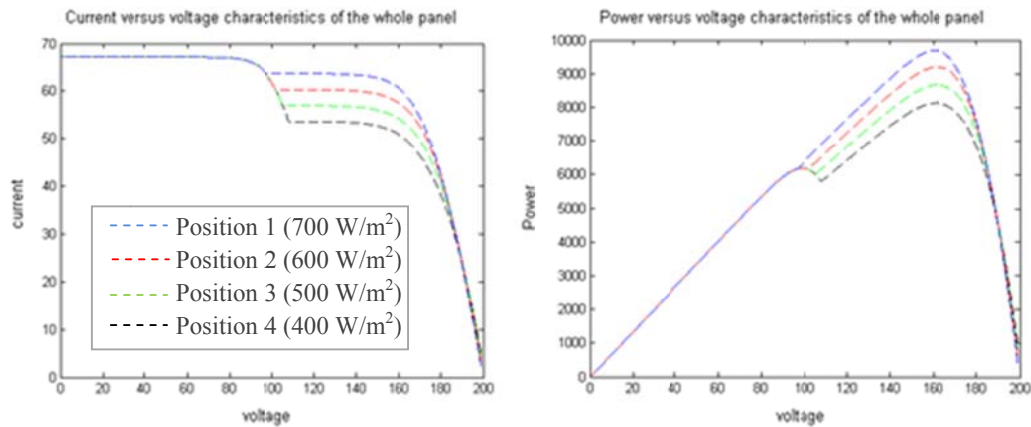
Fig. 25: The I-V & P-V curves of the 10*10 array at each moving position: 1, 2, 3, and 4 of different shading irradiance levels. (Observation 2 scenario-diagonal movement)

The characteristic curves for each shading pattern position are shown in Figure 25. It is obvious that in this observation, the behavior is not the same since the irradiance level of the moving pattern is changing. The global maximum power point was affected here, where it decreased with the decrease of the irradiance level as the shading pattern moved from position 1 to 4. The lower the level of irradiance of the moving shading pattern, the lower is the global maximum power output.

4.4.3. Observation Three

The configuration in observation three (Figure 26) differs from that in observation two in that the whole panel is considered shaded at a level of 400 W/m^2 and the moving shading pattern is of a higher irradiance level, starting from 500 W/m^2 in position 1 and increasing gradually to 800 W/m^2 in position 4 as it moves. In other words, the level of shading decreased (i.e. the level of irradiance increased) as the shading pattern moved from position 1 to 4.The characteristic curves for each shading pattern position are shown in Figure 27. In this observation, the local maximum power

46

point was affected, in which it increased with the increase of the irradiance level as the shading pattern moved from position 1 to 4. The greater the level of irradiance of the moving shading pattern, the greater is the local maximum power output.
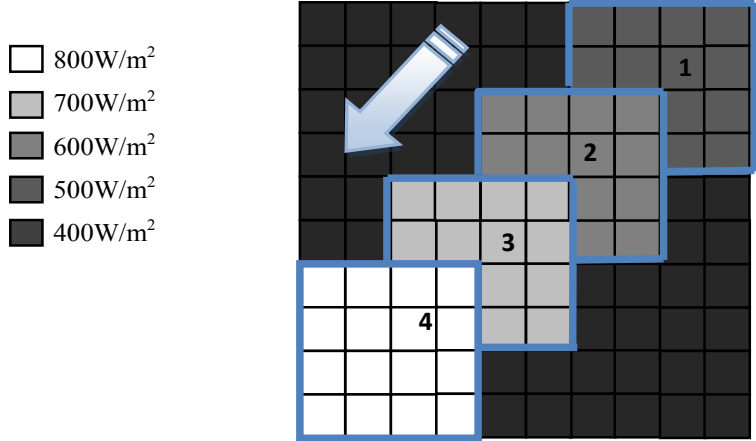

Fig. 26: An array of 10×10 modules at 4 successive moving positions of different shadings. (Observation 3 scenario)
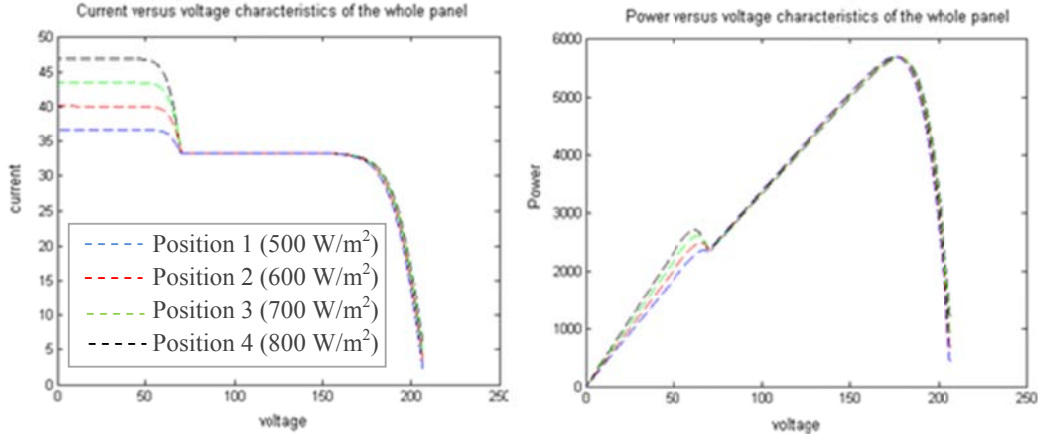

Fig. 27: The I-V & P-V curves of the 10*10 array at each moving position: 1, 2, 3, and 4 of different shading irradiance levels. (Observation 3 scenario)

4.4.4. Observation Four

The configuration in observation four (Figure 28) is the same as that in observation two, but here the movement of the shading pattern is vertical instead of being diagonal, to study the effect of the direction of movement.
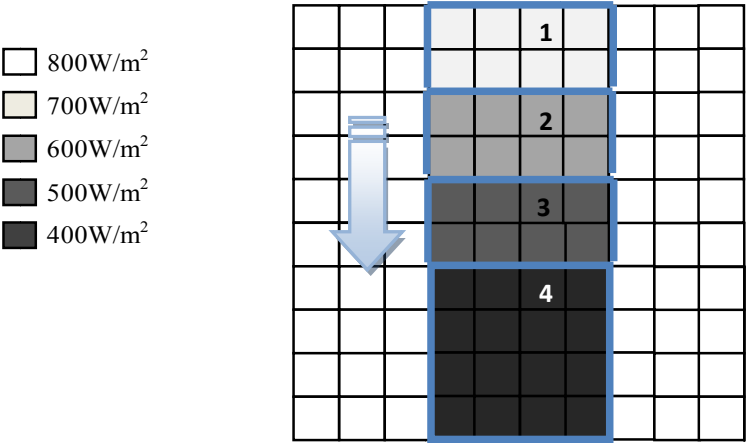
Fig. 28: An array of 10×10 modules at 4 successive moving positions of different shadings. (Observation 4 scenario-vertical movement)
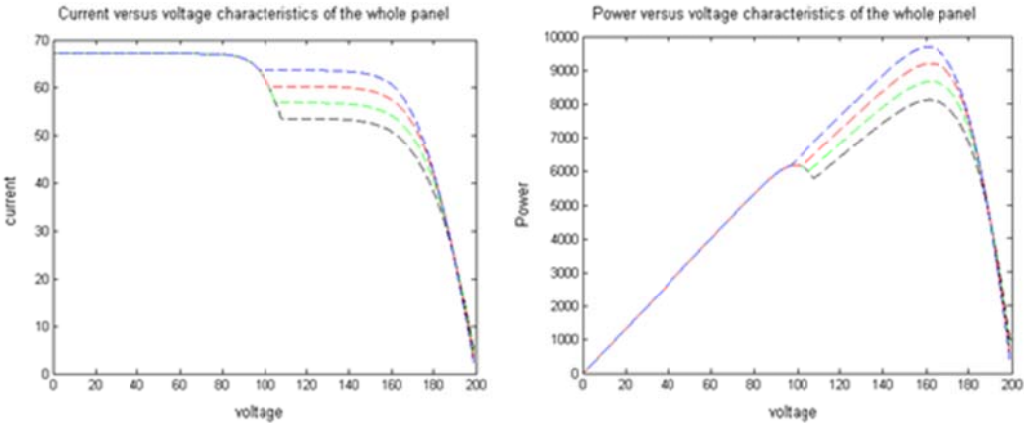
Fig. 29: The I-V & P-V curves of the 10*10 array at each moving position: 1, 2, 3, and 4 of different shading irradiance levels. (Observation 4 scenario-vertical movement)

The characteristic curves for each shading pattern position are shown in Figure 29. The curves are exactly the same as those obtained in observation two. We deduce that the

direction of movement of the shading pattern, whether diagonal or vertical, does not affect the behavior of the panel, as long as the configuration of the groups and the series assemblies in each group is not being changed. In other words, in position 4 for example, Group 2 (whether being in the 1st four columns as in observation two or in the 4th to the 7th columns as in observation four), it is still formed of 4 assemblies and has 2 different irradiance levels (4 modules shaded at 400 W/m^2 and 6 un-shaded at 800 W/m^2 level) in both observations.

4.4.5. Observation Five

Figure 30 shows a PV array consisting of 10 modules in series and with 100 such series-assemblies in parallel.

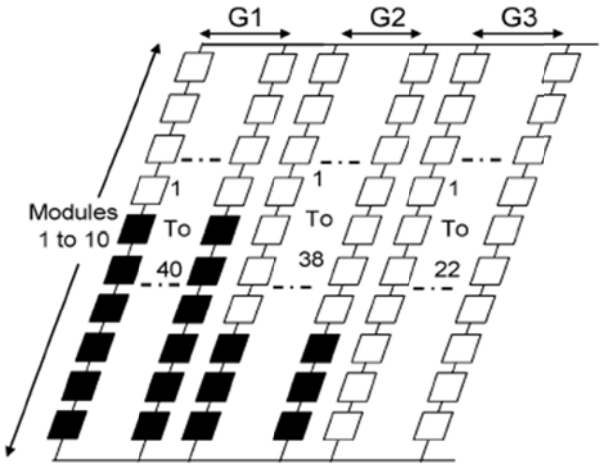Fig. 30: An array of 10×100 modules at 2 different irradiance levels.

Group 1 has 2 different irradiance levels, in which 6 modules are shaded at a level of 100 W/m^2 and 4 modules are un-shaded at a level of 1,000 W/m^2, and is formed of 40 assemblies. Group 2 has also 2 different irradiance levels, in which 7 modules are shaded at a level of 100 W/m^2 and 3 modules are un-shaded at a level of 1,000 W/m^2,

and is formed of 38 assemblies. Group 3 has uniform irradiance and is formed of 22 series-assemblies. The I-V and P-V curves of the whole array under the above described non uniform irradiance pattern are obtained in Figure 31. Figure 32 shows the I-V and P-V curves for a series-assembly from each group.

We deduce that the position of the global peak cannot be generalized to be at the rightmost side of the P-V curve as some approaches assume (mentioned previously in the literature review section). The partial shading configuration shown in Figure 30 is a case where the global peak is in the middle between two local peaks as shown in the P-V curve of Figure 31. Accordingly, the open circuit and short circuit test measurements cannot be applied in the first stage approach to seek for the peak in that region; else the controller would get stuck at a local peak. The main objective is to first estimate the characteristic curves of a certain array configuration, scan the region of the global peak, and then apply the single peak code tracking implemented in the controller to accurately detect the real time maximum point.
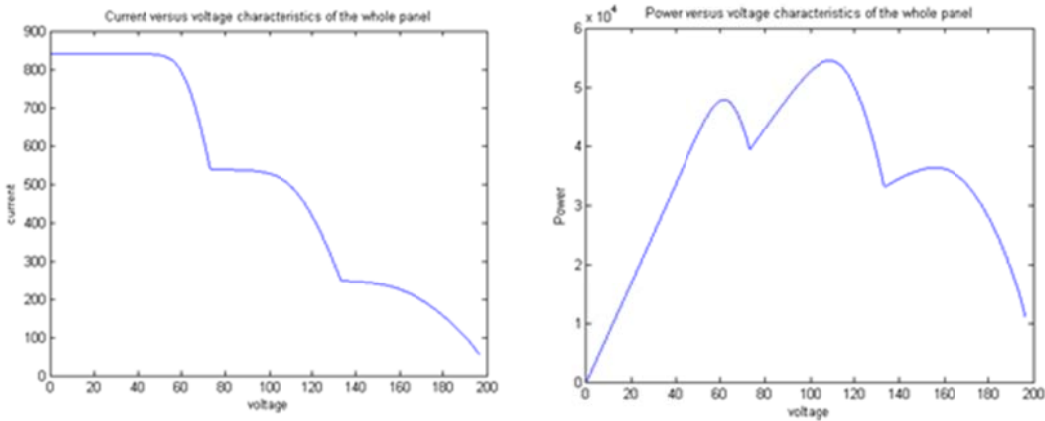

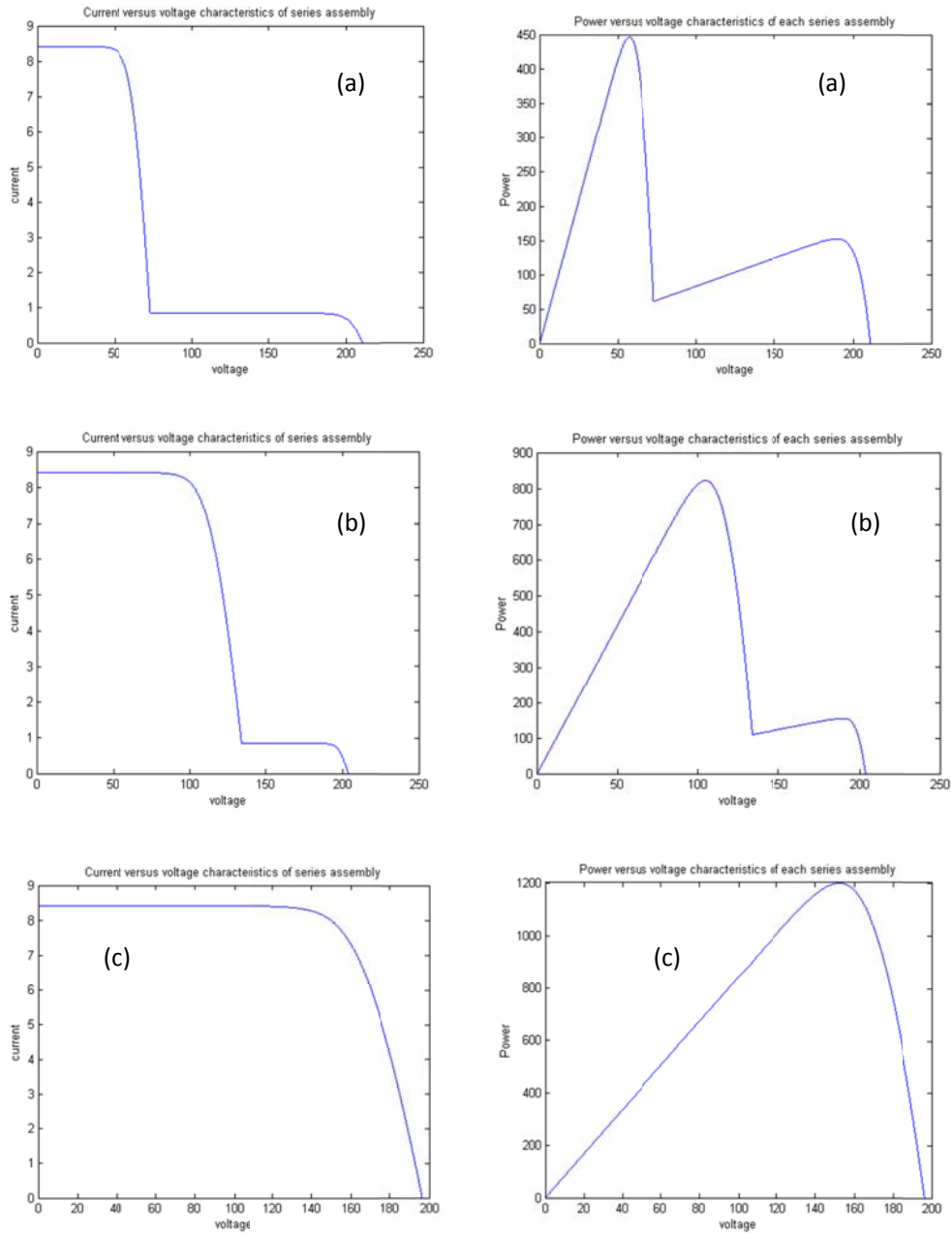Fig. 31: The I-V & P-V curves of the 10*100 array (Observation five)

Fig. 32: The I-V and P-V curves of series-assemblies of observation five.
(a) Group 1. (b) Group 2. (c) Group 3

4.5. Conclusion

As a conclusion to the work presented in this chapter, a MATLAB-based code

has been successfully implemented for modeling and simulating the I-V and P-V

characteristic curves of a PV array under non uniform irradiance due to partial shading. Significant observations that can be deduced are:

- Multiple peaks appear in the characteristic curves as different irradiance levels occur in the shading pattern on the array.
- Series-assemblies with uniform irradiance levels behave as typical single PV modules.
- The number of peaks appearing in a series-assembly characteristic curve is equal to the number of distinct irradiance levels on it.
- The position of the global peak cannot be generalized to be at the rightmost side of the P-V curve. It may be in the middle of local peaks.
- The characteristic behavior of a PV panel is the same no matter where the shading pattern is located on the panel, as long as the shading pattern itself remained the same regarding the irradiance level and the number of modules it covers.
- The lower the level of irradiance of the moving shading pattern, the lower is the maximum power output.
- The direction of movement of the shading pattern, whether diagonal or vertical, does not affect the behavior of the panel, as long as the configuration of the groups and the series assemblies in each group is not being changed.

CHAPTER V

MAXIMUM POWER POINT TRACKING UNDER PARTIAL

SHADING

This chapter presents a novel two-stage approach for tracking the maximum power point of a large PV generator under non-uniform irradiance. As mentioned earlier, the non-uniform irradiance in large PV arrays is attributed to partially shaded PV modules and may significantly increase the complexity of the MPP tracking problem. In Stage 1, the method makes use of real-time irradiance measurements in certain regions of the generator to estimate the power versus voltage curve and to deduce an estimate of the global peak region. Few pyranometers distributed over the modules for the measurement of irradiance levels. The peak of the estimated curve would normally lie in the region of the global peak and makes a good starting operating point for Stage 2. In Stage 2, the single peak tracking approach (explained in chapter III), which combines ripple correlation and incremental conductance, can accurately locate the exact global power point.

5.1. System Components

The system is composed of a set of PV panels charging a battery via a dc-dc boost converter and a MPPT controller, as shown in Figure 33. The panel is composed of 100 PV modules (10 in series modules in each series assembly, and 10 series assemblies in parallel). Each module (represented in a gray shaded box) consists of 36

cells in series with each of an area 0.028 m^2; thus a PV panel of total area around 100 m^2.
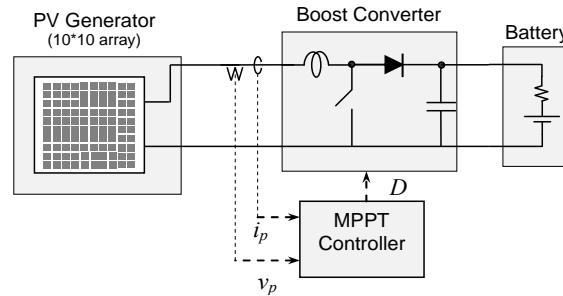
Fig. 33: System model of a PV module charging a battery via a boost converter with an MPPT algorithm implemented.

As shown in Figure 34, a bypass diode is connected in anti-parallel with each PV module when several modules are operating in series, to protect those with low solar irradiance from high power dissipation. The internal capacitance of the modules is being considered in the MPPT tracking algorithm and seems to affect the operation [4, 5]. The per unit area capacitance of a single crystal PV cell at a bias voltage of 0.6 V is approximately 1,000 μF/m^2, so the total capacitance for one module is 0.69 μF [22]. The equivalent capacitance of the whole PV generator is also 0.69 μF, considering 10 capacitances in series and then 10 in parallel.

Fig. 34: Equivalent circuit of a PV module.

5.2. Characteristic Curves Estimation
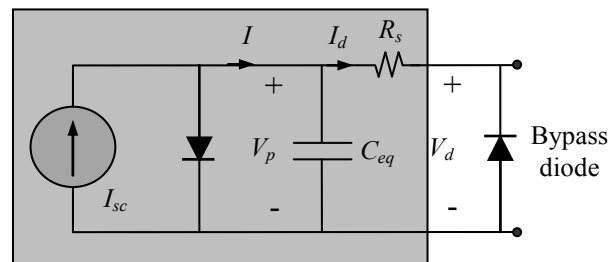
The approach introduced in chapter IV assumes that the irradiance values at each module are inputs, and accordingly computes the P-V curve. However in a real application where the PV generator is significantly large, putting a pyranometer at each module to measure the irradiance is not economical. A solution is to distribute some pyranometers at different regions of the PV generator and use their readings to estimate the irradiance levels at the rest of the modules. Once the estimated irradiance levels are obtained, an approximate P-V curve of the generator may be built by the procedures outlined in the previous chapter. The pyranometers are distributed evenly in a manner to cover the PV generator as uniformly as possible.
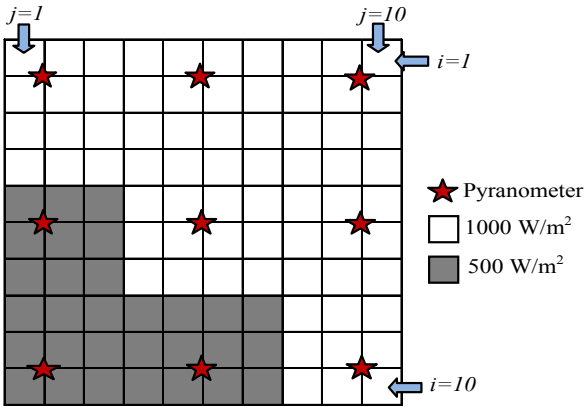
Fig. 35: An array of 10x10 modules with 9 pyranometers.

Figure 35 above shows an example of 9 pyranometers distributed over an array of 10×10 modules. All 4 modules surrounding a pyranometer are assumed to receive the same irradiance level measured by the pyranometer. These modules are indicated by a *flag*=1 so that their irradiance values would not be changed during the estimation process, as shown in Figure 36. A 10×10 array of irradiance values is defined, initialized with negative values for all modules except those in the immediate

neighborhood of a pyranometer. An iterative loop is started, and at each iteration, the modules are scanned starting from the top left module ($i=1, j=1$) in the order of increasing columns (j) within each ascending row (i). The irradiance of each module $G(i, j)$ is updated according to (5.1):

$$G(i,j) = \frac{d_1\, G(i-1,j) + d_2\, G(i+1,j) + d_3\, G(i,j-1) + d_4\, G(i,j+1)}{d_1 + d_2 + d_3 + d_4} \qquad (5.1)$$

where i is the row position of the module, j its column position, and d_i takes the value zero when row i-1 or i+1 or column j-1 or j+1 does not exist (that is when module (i,j) is at the edge of the panel) or when the value G of the corresponding module is still negative and not estimated in the first iteration of estimation. Otherwise d_i is one. Each time, the largest variation in irradiance $\Delta G = G_{new} - G_{old}$ among the whole modules is saved. Iterations end once ΔG is below a defined threshold. In our simulation, we set a threshold of 5 W/m^2. The same process is done for temperature array estimation with a threshold ΔT of 1$^\text{o}$C. Now the irradiance and temperature values fed as input parameters to estimate the PV characteristic of the generator using the procedures described in the previous section.

1000	1000	979	981	1000	1000	998	998	1000	1000
1000	1000	957	965	1000	1000	996	997	1000	1000
849	860	883	924	966	984	990	993	997	998
686	710	793	880	957	982	986	990	996	998
500	500	699	845	1000	1000	982	984	1000	1000
500	500	656	804	1000	1000	957	966	1000	1000
521	545	624	714	804	845	880	924	965	981
519	536	580	624	656	699	793	883	957	979
500	500	536	545	500	500	710	860	1000	1000
500	500	519	521	500	500	686	849	1000	1000

Fig. 36: Estimated irradiance values for each module.

Figure 36 above shows the estimated irradiance values for each module based on the proposed estimation method. The shaded values are those of the modules surrounding a pyrometer and which do not change throughout iterations.
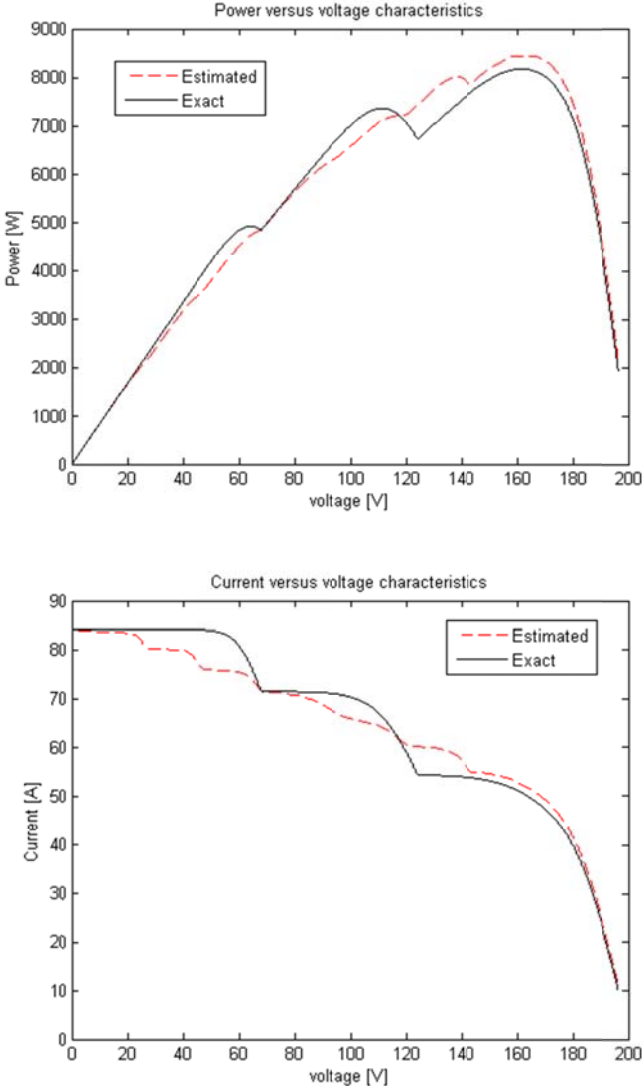

Fig. 37: The estimated and exact P-V and I-V curves for the array configuration

Figure 37 shows the P-V and I-V characteristic curves of the array described in Figure 35. The solid black line is the exact curve assuming that the irradiance values for the whole array are known. The dashed red line is the approximate curve obtained by

estimating the irradiance values from the pyranometers readings using the above

procedure. The estimated curve is smoother due to the averaging approach of the

estimation process, while in the actual shading configuration the irradiance had sharp

jumps from 500 to 1000 W/m^2. The voltage and power values for the estimated global

peak are 163.5 V and 8.45 kW respectively, in comparison to 161.3 V and 8.2 kW

respectively for the actual global peak. It is evident that the estimated global region is a

quite good prediction for setting an initial operating point to start the tracking of the

global peak.

5.3. Global Peak Tracking Algorithm

The curves obtained in Section 5.2 would give an estimate of the global peak

point, which provides an initial operating point to search for the global peak. Then

starting at this estimate, a single MPPT approach is invoked in the controller to detect

the actual global peak. The general approach for tracking a multiple peak PV behavior is

shown in Figure 38 and is described as follows. The pyranometers' measurements are

first read, then the irradiance values of the unmeasured modules are estimated as

described in Section 5.2. The estimated P-V and I-V characteristic curves are then

constructed based on the method presented in Chapter IV. The estimate P-V curve is

scanned and its maximum power point is detected. The voltage, current, and power

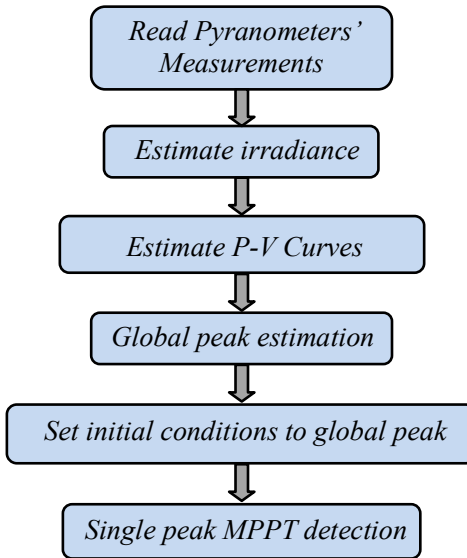values at the corresponding estimated peak are recorded.

Fig. 38: Flow chart showing the general tracking algorithm

Initial operating conditions are defined by setting the boost converter's duty ratio d to a value corresponding to the recorded voltage at the estimated peak as shown in (5.2), where V_{in} is the PV-array output voltage at the estimated peak power point, or the converter input voltage, and V_{out} is the converter's output voltage or the battery voltage:

$$d = 1 - \frac{Vin}{Vout} \tag{5.2}$$

After setting the initial operating conditions in a region near to the GP, the tracking issue now reduces to a single peak tracking situation. The new single peak code [7] presented in a Chapter III is used in this simulation. The approach makes use of both methods: IC and RCC. The error of the actual operating point at each sampling time is calculated based on the fundamental concept of IC, namely that $\Delta P/\Delta V$ at the MPP is zero. However, the method does not evaluate the changes in the current and voltage

values from the present and previous samples as in the IC approach. Instead, it makes use of the PV array inherent current and voltage ripples caused by the boost converter without artificial and intentional perturbation at each sampling time.

The characteristic I-V curve of the PV array is not given by an analytical expression as in the case of a single module (4.3). So for the purpose of simulating the real time behavior of the PV generator, the exact curves are computed and a look up table is created within the software simulation. In case of hardware simulation, the currents and voltages are directly measured in real-time.

5.4. Multiple Peaks Tracking Results

Two different possible cases of shading are examined for simulation. For each case, power peak tracking was done by two approaches, the first without estimating the global region and the second by introducing the GP region detection for setting initial conditions near the actual peak power point.

5.4.1. Case One

The array is initially subjected to uniform irradiance (400 W/m^2) and consequently a single power peak would appear in the characteristic curves. Then at 0.01s, the irradiance is increased to 800 W/m^2 in the top 7 rows of the array, as shown in Figure 39. With this non-uniform irradiance, two peaks would appear and the need for a method that successfully tracks the GP instead of a local one becomes essential. Figure 40 shows the characteristic P-V curves under uniform and non-uniform irradiance. At uniform irradiance, the curves marked in dashed black show a single peak in the P-V curve. However, at non uniform irradiance, two peaks appear in the P-V

curve marked with a green dashed line; one of them is the global peak operating point
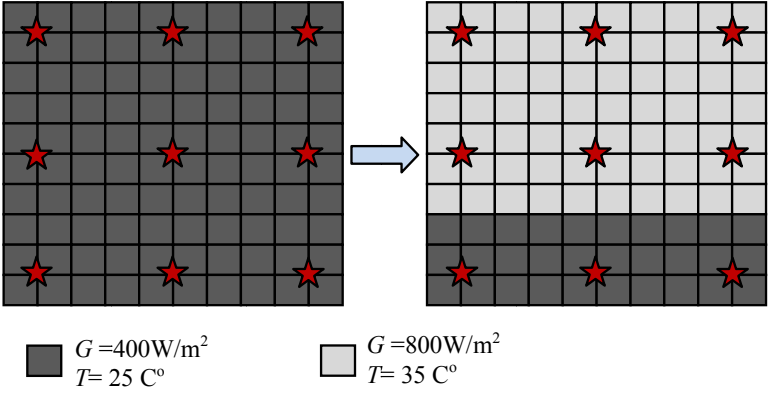
being sought.

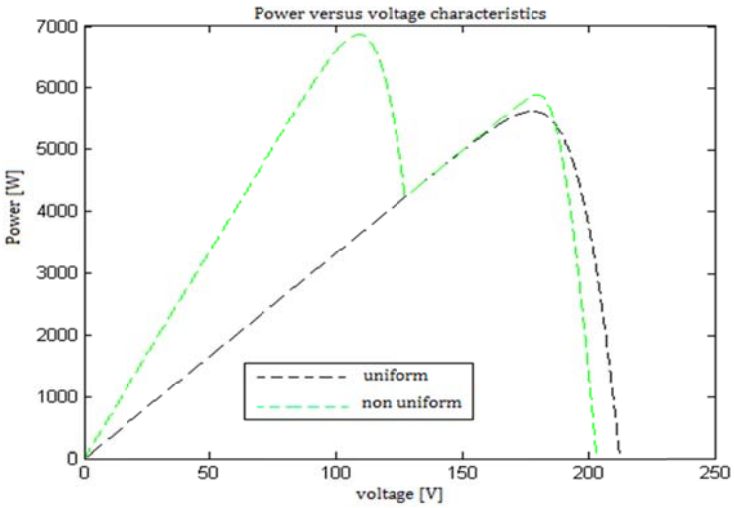Fig. 39: Partial shading configuration of case one.

Fig. 40: P-V characteristic curves of case 1 in the two states.

Tracking without GP Estimation: Under uniform irradiance, the tracking is

straightforward as there is one single peak to track. When the starting point is set at

V_{array} = 150 V, I_{array} = 33.3 A, and duty cycle d=0.25, the GP is reached with V_{array} =

176.4 V, P_{array} = 5,610 W and d=0.16. After the sudden change detected in the readings

of the pyranometers leading to partial shading, the system starts at the voltage

conditions of the previous peak, which is now in the region of the local peak of the new

state as shown in the P-V curve of Figure 40, and reaches the local peak of $V_{array} = 185$

V, $P_{array} = 5,820$ W and $d=0.075$. So without GP region estimation, the simulation will

fail to reach the global peak that lies rather to the left. Figure 41 shows that tracking
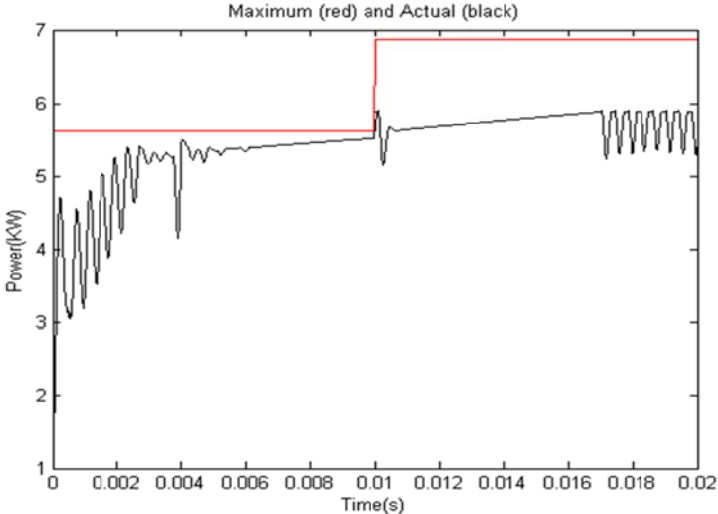
failed to detect the actual maximum peak.

Fig. 41: Tracking case one without GP region Estimation.

Tracking with GP Estimation: After the sudden change, the irradiance

values for the array modules are predicted based on the linear averaging method of the 9

pyranometers readings. The estimated I-V curve of the array is then constructed and its

peak power point is noted, which forms an estimate of the GP. The duty cycle is set to a

new value corresponding to the estimated GP and the tracking starts from there and

succeeds to reach the actual maximum peak, as shown in Figure 42.

Under uniform irradiance, the initial estimated conditions are: $V_{array} = 178$ V,

$I_{array} = 31.5$ A, and a duty cycle $d=0.15$ and the final operating points at the MPP is:

V_{array} = 176.4 V, I_{array} = 31.8 A, P_{array} = 5.61 kW and duty cycle d=0.16. After the

sudden change, the estimated initial conditions are: V_{array} = 115 V, I_{array} = 54.6 A, and a

duty cycle d=0.45; the final operating point at the MPP is: V_{array} = 108.6 V, I_{array} = 63.15

A, P_{array} = 6.85 kW and a duty cycle d=0.48. In both states, the estimated initial
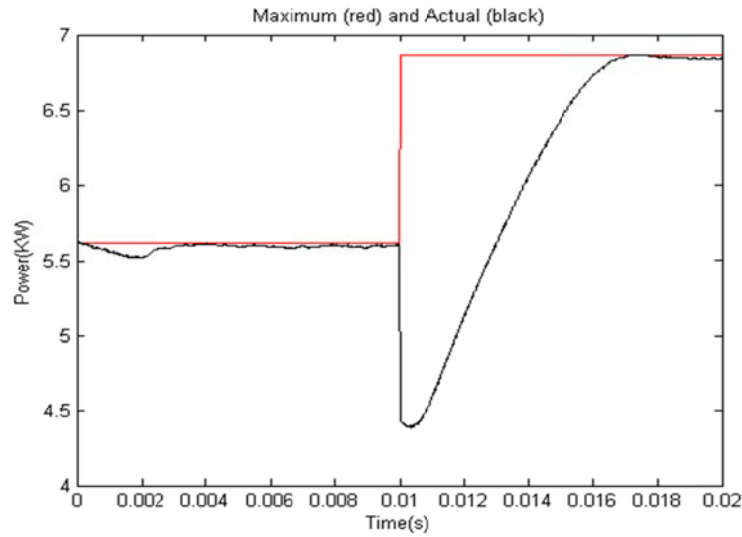
operating voltage is in the region of the actual GP.

Fig. 42: Tracking case one with a prior GP region estimation

5.4.2. Case Two

In case two, the array was initially subjected to partial shading 800 W/m² for

the first 7 rows and 400 W/m² for the bottom 3 rows (State 1). Then at half of the

simulation time, the irradiance levels of the top 7 rows of the array decreased to 600

W/m² (State 2). This is illustrated in Figure 43.

Figure 44 below shows the P-V characteristic curves of the two states. This is

another typical case where the region of the global peak completely changes with a
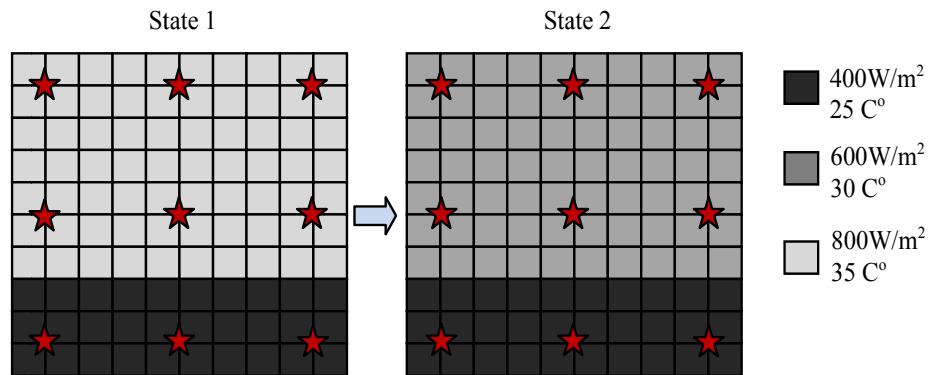
shading configuration change.

Fig. 43: Partial shading configuration of case two.
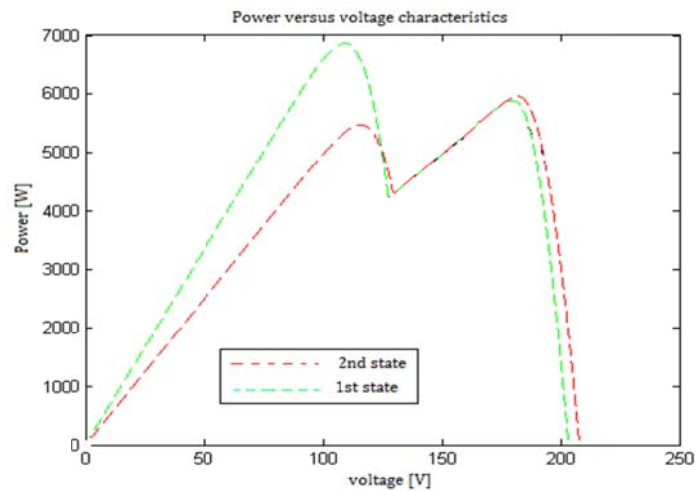
Fig. 44: P-V curves of case 2 in the two states.

Tracking without GP Estimation: When the system is initially in State 1 its MPP is reached at: $V_{array} = 107.9$ V, $P_{array} = 6{,}850$ W and duty cycle $d=0.48$; the search is started from an estimated point at $V_{array} = 115$ V, $P_{array} = 6{,}210$ W, and duty cycle $d=0.44$; this is shown in the first part of Figure 45. When the irradiance and temperature change they cause a complete shift in the GP region, and so the continued tracking brings the system to the local peak of $V_{array} = 120$ V, $P_{array} = 5400$ W and duty cycle

d=0.4 shown in the P-V curve of Figure 44. The failed tracking in the time domain to detect the GP of State 2 is illustrated in the second part of Figure 45.
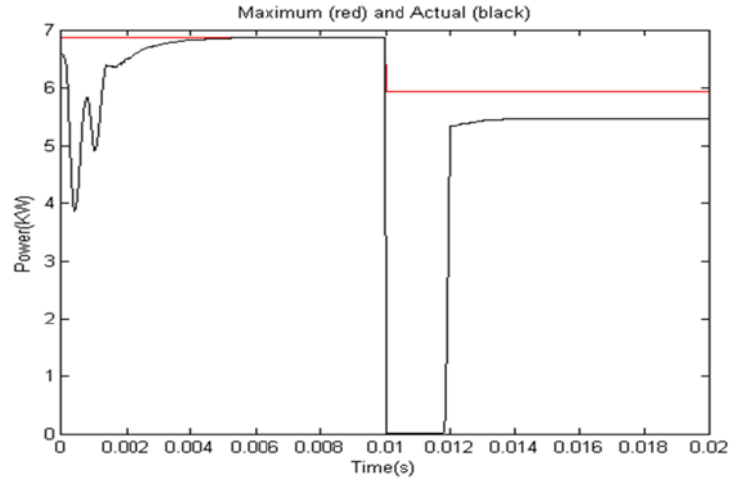
Fig. 45: Tracking case two without GP estimation.

Tracking with GP Estimation: In this mode, the irradiance values are predicted based on the linear averaging method starting from the readings of the 9 pyranometers. The peak of the estimated curve is then noted to be V_{array}= 182V, P_{array} = 6,005 W and *d*= 0.14. When tracking resumes from this point, the final operating points at the MPP is reached at: V_{array}= 180.5 V, P_{array}= 5,920 W and duty cycle *d*=0.15. Tracking from the estimated peak in this case again succeeds in reaching the actual GP, as shown in Figure 46 below. In both states, the initial operating voltage is in the region of the actual GP.

Fig. 46: Tracking case two with a prior GP region estimation.

CHAPTER VI

CONCLUSION AND FUTURE WORK

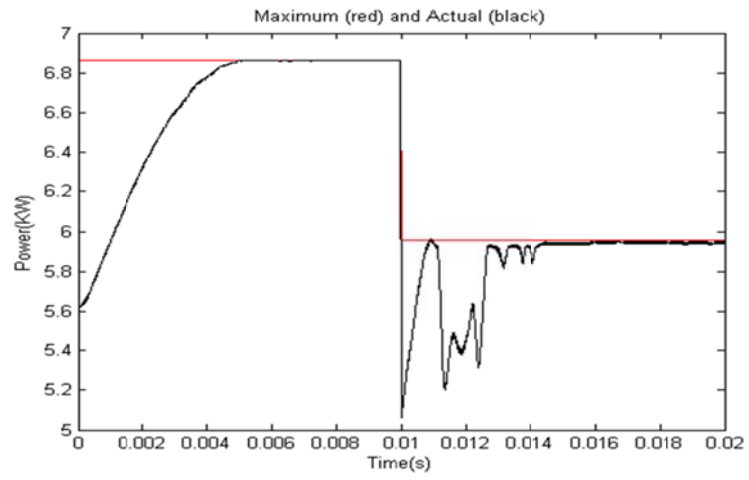## 6.1. Concluding Remarks

This thesis has presented a detailed, new, single peak MPPT approach. It uses the fundamental concept of incremental conductance to seek the MPP. The method presented does not evaluate the changes in the current and voltage values from the present and previous samples as in the IC method. Instead, it makes use of the inherent current and voltage ripples caused by the boost converter to compute the error and change the duty cycle accordingly without additional perturbation at each sampling time. The models of the different system components and the control methodology were presented and discussed. The simulation was based on the IT method for solving the DE of system, which is known for its stability. The tuning of the associated PID controller was carried out to drive the error to zero in a fast and effective way. The effectiveness of the proposed method was verified by simulation results that showed successful, high efficiency of tracking towards the maximum power point under various, rapidly changing irradiance levels.

This thesis presented also a novel two stage method for tracking multiple power peaks that occur in case of partial shading. An approach was proposed to build the characteristic curves of a large array of series and parallel connected modules. Then from pyranometer measurements suitably distributed on the array, the irradiance values for the whole array are estimated using an iterative averaging procedure. The tracking algorithm makes use of the estimated irradiance values to construct an estimate of the P-V curves which set the initial point of tracking when sudden changes occur. Simulation

results have shown successful tracking towards the maximum peak, and demonstrated the importance of estimating the GP region to avoid getting stuck in local peaks. The advantage of this method is that it does not perturb the operation by carrying out open circuit and short circuit tests in trying to localize the global peak.

6.2. Future Work

Future work in the same field of this thesis is concentrated on hardware implementations. Implementing the design on hardware, for both a single PV module under uniform irradiance and a large PV array under partial shading, to check for accurate peak tracking, to run several cases, and to find out the system's efficiency is quite essential. The future work may extend to verify simulation results by testing the results, analyzing them, measuring the tracking efficiency, and comparing it with other approaches. This is expected to be operational as it was verified in simulation. Also future work scope may extend to compare between real shading characteristics and the approximated ones. The challenges would be to study:

- the criteria of distributing the pyranometers effectively across the panel
- the accuracy of the estimated shading pattern
- the accuracy of the first stage global peak estimation
- possibility of the model detecting a global peak estimation in the local peak region
- the effect of distribution of the pyranometers on the accuracy

Moreover, introducing the notion of delay between the times the voltage and current measurements are taken and between the times they effectively reach the MPPT controller would be a quite good simulation for the real time behavior of tracking.

Current and future work in MPPT is focusing more on two-stage MPPT to track the MPP of multiple arrays. The only main challenge that remains to prove the effectiveness of the new approach presented in this thesis is to provide hardware results that verify the results obtained from the simulation studies.

REFERENCES

[1] M. Serhan, S.H. Karaki, and L.R. Chaar, "An adaptive perturb and observe maximum power point tracking system of photovoltaic arrays," *International Solar Energy Conference 2005* (*ISEC* 2005), paper no. 76251, pp. 515-522

[2] J. Jiang, T. Huang, Y. Hsiao, and C. Chen, "Maximum power tracking for photovoltaic power systems," *Tamkang Journal of Science and Engineering*, Vol. 8, no. 2, 2005, pp. 147-153

[3] K.H. Hussein, I. Muta, T. Hoshino, and M. Osakada, "Maximum photovoltaic power tracking: an algorithm for rapidly changing atmospheric conditions", *IEE Proceeding on Generation Transmission and Distribution*, vol. 142, no. 1, January 1995.

[4] T. Esram, J.W. Kimball, P.T. Krein, P.L. Chapman, P. Midya, "Dynamic maximum power point tracking of photovoltaic arrays using ripple correlation control," *IEEE Transactions on Power Electronics*, vol. 21, no. 5, September 2006, pp. 1282-1291

[5] J. W. Kimball, P. T. Krein, "Discrete-Time ripple correlation control for maximum power point tracking," *IEEE Transactions on Power Electronics*, vol. 23, no. 5, September 2008, pp. 2353-2362

[6] H. Patel, V. Agarwal, "MATLAB-Based Modeling to Study the Effects of Partial Shading on PV Array Characteristics," *IEEE Trans. on Energy Conversion*, vol. 23, no.1, pp. 302-310, March 2008.

[7] F. Kazan, S. Karaki, R. Jabr, M. Mansour, "Maximum Power Point Tracking Using Ripple Correlation and Incremental Conductance," *47th International Universities' Power Engineering Conference*, September 2012.

[8] D. Sera, R. Teodorescu, J. Hantschel, M. Knoll, "Optimized Maximum Power Point Tracker for Fast-Changing Environmental Conditions," IEEE Transactions on Industrial Electronics, Vol. 55, no. 7, July 2008, pp. 2629-2637.

[9] A. Pandey, N. Dasgupta, A. K. Mukerjee, "Design Issues in Implementing MPPT for Improved Tracking and Dynamic Performance," *IEEE Conference*, 2006.

[10] F. Liu, S. Duan, F. Liu, B. Liu, Y. Kang, "A Variable Step Size INC MPPT Method for PV Systems," *IEEE Transactions on Industrial Electronics*, Vol. 55, no. 7, July 2008, pp. 2622-2628.

[11] K. S. M. Raza, H. Goto, O. Ichinokura, H. Guo, "An Improved and Very Efficient MPPT Controller for PV Systems subjected to Rapidly Varying Atmospheric Conditions and Partial Shading," Tohoku University, Japan.

[12] Q. Mei, M. Shan, L. Liu, J. M. Guerrero, "A Novel Improved Variable Step-Size Incremental-Resistance MPPT Method for PV Systems," *IEEE Transactions on Industrial Electronics*, Vol. 58, no. 6, June 2011, pp. 2427-2434.

[13] K.P. Kroeger, S. Choi, A. M. Bazzi, B. B. Johnson, P. T. Krein, "A Digital Implementation of Continuous-time Ripple Correlation Control for Photovoltaic Applications," *IEEE Conference*, 2010

[14] G. Walker, "Evaluating MPPT converter topologies using a MATLAB PV model," *J. Electr. Electron. Eng. Aust.*, vol. 21, no. 1, 2001, pp. 49–56.

[15] M. C. Alonso-Gracia, J. M. Ruiz, and F. Chenlo, "Experimental study of mismatch and shading effects," *Solar Energy Mater. Solar Cells*, vol. 90, no. 3, Feb. 2006, pp. 329–340.

[16] H. Kawamura, K. Naka, N. Yonekura, S. Yamanaka, H. Kawamura, H. Ohno, and K. Naito, "Simulation of I–V characteristics of a PV module with shaded PV cells," Solar Energy Mater. Solar Cells, vol. 75, no. 3/4, Feb. 2003, pp. 613–621.

[17] H. Patel, V. Agarwal, "Maximum Power Point Tracking Scheme for PV Systems Operating Under Partially Shaded Conditions," *IEEE Transactions on Industrial Electronics*, Vol. 55, No. 4, pp. 1689-1698, April 2008.

[18] K. S. M. Raza, H. Goto, O. Ichinokura, H. Guo, "An Improved and Very Efficient MPPT Controller for PV Systems subjected to Rapidly Varying Atmospheric Conditions and Partial Shading," *19th Australasian Universities Power Engineering Conference*, pp.1-6, 2009.

[19] K. Kobayashi, I. Takano, Y. Sawada, "A Study on a Two Stage Maximum Power Point Tracking Control of a Photovoltaic System under Partially Shaded Insolation Conditions," *IEEE Power Engineering Society General Meeting,* pp. 2612-2617, 2003.

[20] A. Bazzi, S. Karaki, "Simulation of a New Maximum Power Point Tracking Technique for Multiple Photovoltaic Arrays," *IEEE Int. Conference on Electro/Information Technology*, pp. 175-178, 2008.

[21] H. Taheri, Z. Salam, K. Ishaque, K. Syafaruddin, "A Novel Maximum Power Point Tracking Control of Photovoltaic System Under Partial and Rapidly Fluctuating Shadow Conditions Using Differential Evolution," *IEEE Symposium on Industrial Electronics and Applications*, 2010.

[22] C.R. Jeevandoss, M. Kumaravel, V. Jagadeesh Kumar, "A novel method for the measurement of the C-V characteristic of a solar photovoltaic cell", *IEEE Instrumentation and Measurement Technology Conference*, May 3-6, 2010, pp.371-374.

[23] N. Mohan, T. Undeland, W. Robbins, *Power electronics: Converters, Applications and Design*, New Jersey: JohnWilley & Sons, 1989.

[24] J. Arrillaga and C.P. Arnold, *Computer analysis of power systems*, Chichester, England: Wiley, 1990, pp. 182-184.